energies

MDPI

Article

Power System Stability Analysis of the Sicilian Network in the 2050 OSMOSE Project Scenario †

James Amankwah Adu [1], Alberto Berizzi [2,*], Francesco Conte [3], Fabio D'Agostino [3], Valentin Ilea [2], Fabio Napolitano [1], Tadeo Pontecorvo [1] and Andrea Vicario [2]

[1] Department of Electrical, Electronic and Information Engineering, University of Bologna, 40126 Bologna, Italy; jamesamankwah.adu@unibo.it (J.A.A.); fabio.napolitano@unibo.it (F.N.); tadeo.pontecorvo@unibo.it (T.P.)
[2] Department of Energy, Politecnico di Milano, 20156 Milan, Italy; valentin.ilea@polimi.it (V.I.); andrea.vicario@polimi.it (A.V.)
[3] Department of Electrical, Electronics and Telecommunication Engineering and Naval Architecture, University of Genoa, 16145 Genoa, Italy; fr.conte@unige.it (F.C.); fabio.dagostino@unige.it (F.D.)
* Correspondence: alberto.berizzi@polimi.it
† This paper is an extended version of our paper published in 2021 AEIT International Annual Conference (AEIT), Milano, Italy, 4–8 October 2021; pp. 1–6.

Abstract: This paper summarizes the results of a power system stability analysis realized for the EU project OSMOSE. The case study is the electrical network of Sicily, one of the two main islands of Italy, in a scenario forecasted for 2050, with a large penetration of renewable generation. The objective is to establish if angle and voltage stabilities can be guaranteed despite the loss of the inertia and the regulation services provided today by traditional thermal power plants. To replace these resources, new flexibility services, potentially provided by renewable energy power plants, battery energy storage systems, and flexible loads, are taken into account. A highly detailed dynamical model of the electrical grid, provided by the same transmission system operator who manages the system, is modified to fit with the 2050 scenario and integrated with the models of the mentioned flexibility services. Thanks to this dynamic model, an extensive simulation analysis on large and small perturbation angle stability and voltage stability is carried out. Results show that stability can be guaranteed, but the use of a suitable combination of the new flexibility services is mandatory.

Keywords: large perturbation angle stability; small perturbation angle stability; voltage stability; synthetic inertia; demand response; reactive compensation

Citation: Adu, J.A.; Berizzi, A.; Conte, F.; D'Agostino, F.; Ilea, V.; Napolitano, F.; Pontecorvo, T.; Vicario, A. Power System Stability Analysis of the Sicilian Network in the 2050 OSMOSE Project Scenario. *Energies* **2022**, *15*, 3517. https://doi.org/10.3390/en15103517

Academic Editor: Saeed Golestan

Received: 30 March 2022
Accepted: 5 May 2022
Published: 11 May 2022

1. Introduction

The energy transition process will lead the penetration of Renewable Energy Sources (RESs) in the European power system to drastically increase. In a few decades, traditional generation plants will be progressively decommissioned, and their fundamental contribution to the power system flexibility will be missed. Flexibility is understood as the power system's ability to cope with variability and uncertainty in demand and renewable generation over different timescales to guarantee a stable and efficient operation [1]. Therefore, the challenge is to keep the current level of power system flexibility by exploiting a new mix of resources, i.e., the same RESs, but also loads by Demand Side Response (DSR) and energy storage systems.

Academic and industrial research studies have been (and are) extensively active in proposing methods and technologies able to transform RESs and loads into sources of flexibility by modifying their control procedures and/or combining them with Battery Energy Storage Systems (BESSs). More specifically: in [2–4] the authors propose control strategies to enable wind generators to provide Synthetic Inertia (SI); in [5] wind generators are made capable to provide primary droop frequency regulation; in [6,7] converter-interfaced generators are designed to provide SI; in [8–10] aggregates of thermal loads are controlled

to provide primary and secondary frequency regulation services; in [11] a control strategy for a building air cooling system that provides secondary frequency regulation is experimentally validated; in [12] multiple BESSs are controlled to provide frequency regulation; in [13] BESSs are coupled with wind generators to provide frequency regulation services; in [14] a BESS is coupled with a large scale photovoltaic (PV) generator to provide primary frequency regulation; in [15] a decentralized control strategy is proposed to allow wind generators to provide primary voltage regulation; in [16] primary voltage regulation is realized by multiple BESSs via broadcast control at subtransmission level, while [17] generalizes this technique for any type of RES, applies it at distribution network level, upgrades it with an additional coordination level and compares it against centralized optimal reactive power control; in [18,19] voltage regulation is realized through DSR considering residential loads; in [20] voltage regulation performance form Distributed Energy Resources (DERs) are validated by Hardware-in-the-Loop simulations; in [21,22] voltage regulation is realized by PV generators; in [23] a chance-constrained optimization method is proposed to provide voltage regulation by DERs; in [24] voltage regulation is provided by distributed BESSs via reinforcement learning.

To summarize, the result is a huge collection of possible solutions by which the new mix of resources can provide several classes of flexibility, such as SI, support to frequency, voltage regulation, and balancing services.

In this context, the European project OSMOSE [25–27] has the objective of defining the optimal mix of flexibility resources among all the available options in order to avoid stand-alone solutions that might be less efficient in terms of overall efficiency. The project, involving nine European countries, three Transmission System Operators (TSOs), many companies, universities, and research institutions, covers several aspects to evaluate flexibility needs and assess flexibility services.

In this paper, we focus on Stability Aspects within the scope of the work performed by EnSiEL [28] under Task 1.4.3. More specifically, the Work Package 1 (WP1) of the project started with Task 1.1, led by the Technical University of Berlin (TUB), by proposing long-term future scenarios for the years 2030 and 2050 [25], which differ in load levels, installed capacities, investment possibilities, and the quantity of flexibility options. Next, Task 1.2 (carried out by RTE, the French TSO) assessed and validated these scenarios [27,29] using a static reserve adequacy analysis. Finally, in Task 1.4.3, EnSiEL evaluated the impact of innovative flexibility sources on the power system stability, testing these scenarios for 2030 and 2050 in a realistic model of the electrical network of Sicily. Sicily, one of the two main islands of Italy, is synchronously connected to the national power system. The grid model was provided by Terna, the Italian TSO.

Since results for 2030 were briefly presented in [30], this paper focuses on the 2050 scenario. In particular, we evaluate the response of the power system to some typical perturbations (e.g., loss of a large generator, slow increase in loads, and contingencies of branches) by simulations carried out on the DIgSILENT PowerFactory 2019 platform [31].

According to the 2050 scenario, the flexibility sources considered in this analysis are:

- SI provided by wind generators;
- FFR provided by BESSs;
- SI and FFR provided by controlled loads (DSR);
- Voltage regulation support provided by RESs (PV and wind generators).

The following topics are investigated:

1. *Large-perturbation angle stability (electromechanical stability)*: To analyze the response of the power system to the variations in frequency and voltage on a time scale from tens of milliseconds up to tens of seconds. In particular, the electromechanical stability is assessed, taking into account the dynamics of generators and loads and the triggering of protection schemes. The objective is to state if synchronous machines can keep synchronism after a severe transient disturbance [32].

2. *Small-perturbation angle stability*: To evaluate the power system stability when small variations in loads and generation occur, as continuously happens in a real scenario, not necessarily related to a transient disturbance.
3. *Voltage security*: To assess the capability of a power system to keep an acceptable steady voltage at all busses, either under normal conditions or after disturbances.

The results prove that in the 2050 scenario, with an extremely high penetration of RESs, the new flexibility sources are essential to guarantee both angle and voltage stability. Literature provides many works with power system stability analyses taking into account the lowering of the system inertia [33] and the high penetration of inverter-based generation [34,35]. However, in most cases, these studies focus on one or two stability issues and simulation tests are carried out on relatively small (less than one hundred busses) benchmark network models. Differently, this paper proposes an original and useful analysis which:

- Is based on validated realistic scenarios for the year 2050;
- Takes into a complete set of flexibility options, as listed before (SI provided by wind generators; FFR provided by BESSs; SI and FFR provided by controlled loads (DSR); voltage regulation support provided by RESs);
- Uses a detailed network model composed by more than 600 busses, provided by the TSO that owns and manages the modeled system.

The reminder of the paper is organized as follows. Section 2 describes the network model and the simulation scenarios. Section 3 presents the results of the large perturbation stability analysis. Section 4 reports the results of the small-perturbation stability analysis. Section 5 presents the results of the voltage stability analysis. Finally, Section VI provides the general conclusions of the study.

2. Network Model and Scenarios

The grid model employed for this analysis is the Sicilian Island, a portion of the Italian transmission network (Figure 1); basic data were provided by Terna.

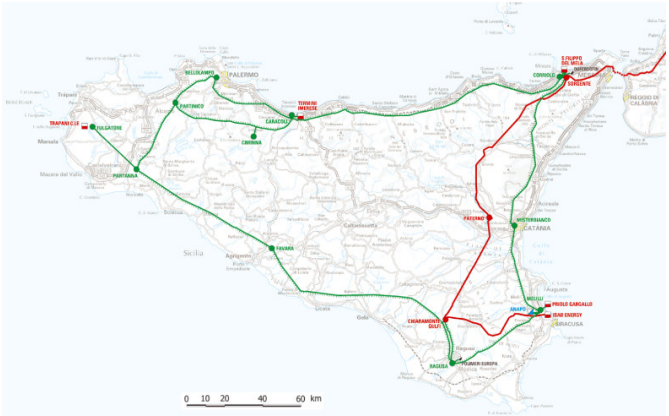

Figure 1. The studied grid [36].

The Sicilian Island corresponds to the European market zone 56IT used by Task 1.1 and 1.2 of the OSMOSE project [25,29]. The provided grid model is detailed and presents:

1. More than 600 busbars at 400, 230, 150, and 132 kV;
2. 441 lines;
3. 516 substations;
4. 30 large (nominal power higher than 10 MW) static generators, representing the wind and solar plants connected to the HV grid;
5. 379 loads, mimic both equivalents and HV loads;
6. 72 synchronous machines representing both thermal and hydro plants with their associated controllers.

The grid presents only few lines with a voltage higher or equal to 230 kV (in green in Figure 1); considering the geographic dimension and the high amount of generation capacity installed, it is poorly meshed. The 400 kV system (in red in Figure 1) essentially consists of a single backbone starting from the Sorgente substation in the north-east and ending in the Syracuse petrochemical nucleus in the south-eastern part of the region. It goes through the powerful interconnection substations of Sorgente, Paternò, and Chiaramonte Gulfi up to the ISAB plants near Priolo Gargallo. Since 2016, Sicily has been connected to the Italian system through a new AC interconnection (two parallel undersea cables) at 400 kV. Both the AC interconnections start from Rizziconi substation on the mainland and get to the Sorgente substation on the Island.

Regarding the installed conventional generators, Table 1 reports Sicily's major thermal power plants in 2020.

Table 1. Sicily's major thermal power plants in 2020.

Plant	Owner	Type	Rating (MW)
Anapo (SR)	Enel	Storage Hydro	500
Augusta (SR)	Enel	Fossil Fuel	210
Priolo Gargallo, Nuce Nord (SR)	ERG	CCGT *	480
Priolo Gargallo, ISAB energy (SR)	ERG	IGCC *	528
Priolo Gargallo Archimede (SR)	Enel	CCGT	750
Trapani (TP)	E.On	OCGT *	169
Gela (CL)	Eni	Fossil Fuel	260
San Filippo del Mela (ME)	A2A Energie Future	Fossil Fuel	1280
Milazzo (ME)	Termica Milazzo	CCGT	365
Termini Imerese (PA)	Enel	CCGT	1340

* CCGT—Combined Cycle Gas Turbine, IGCC—Integrated Gasification Combined Cycle, OCGT—Open Cycle Gas Turbine.

As mentioned, all conventional generators provide droop primary frequency regulation (by the governor), primary voltage regulation (by the Automatic Voltage Regulator), and Power System Stabilizers (PSS). In this paper, focusing on frequency regulation, we indicate the primary active power reserve as Frequency Containment Reserve (FCR) according to the nomenclature introduced in [37].

In the Rizziconi substation, end of the link in the continent, a frequency relay is installed; it is able to disconnect the Island from the rest of the system in particular critical conditions. Usually, Sicily exports to Italy active power, keeping the Sicilian power system in operation in case of the trip of the interconnection and avoiding load shedding on the Island. Active power transit is always monitored, and if the exported power is higher than a given amount, specific devices can disconnect some generators in Sicily.

Moreover, the Rizziconi–Sorgente Islanding relay trips when severe underfrequency events occur in the continental power system; the tripping relay operates according to these rules:

- The frequency overtakes the threshold of 49.7 Hz and the frequency derivative is lower than -0.2 Hz/s;
- The frequency is lower than 49.5 Hz.

These rules also explain why Sicily mainly exports power; indeed, in case of an underfrequency event, if the Island was importing, a disconnection could worsen the frequency decay. Sicilian four large pumping units of Anapo plant are always disconnected as a first solution if operating in pumping mode.

In the case of underfrequency events, moreover, a load shedding scheme is in operation, where its settings are shortly described in Table 2: according to different thresholds, a prescribed load shedding step is activated, as described.

Table 2. Load shedding settings [38].

Threshold	Starting Frequency (Hz)	Frequency Derivative Threshold (Hz/s)	Pure Frequency Threshold (Hz)	Percentage of Shed Load
1	49.3	−0.3	49.0	9%
2	49.2	−0.6	48.9	8%
3	49.1	−0.9	48.8	7%
4	49.1	−1.2	48.7	7%

2.1. Scenarios

2.1.1. Data Scenario Application

The scope of this work is to simulate the dynamical stability of the Sicilian grid with a different mix of loads and generation deployment (coming from Task 1.1 and Task 1.2) and evaluate possible security issues and possible suggestions for countermeasures. The Sicilian grid has been updated with the new values of capacities and loads identified for 2050. Each scenario identified in Task 1.1 provides data for the 99 European zones defined by e-Highway 2050. In detail, for each zone, the total installed generation capacity, differentiated by primary sources (biomass, geothermal, wind, solar, gas, and hydro), is given, as well as the total load installed.

Task 1.1 provided the installed capacity, differentiated by technology, for each European market zone, either connected to the HV or MV grids. This new capacity was allocated to the HV and MV grids, according to the 2020 shares available on the GAUDÌ portal [39], the Terna's website with the technical characteristics of all the power plants. Table 3 shows the RES deployment in Sicily (2020) and the percentage connected to either MV or HV level; it is clear that the PV plants are almost always connected to the distribution grid, and the wind and hydro plants to the transmission grid. Such percentages were used to share the RES data provided by Task 1.1, while some conventional thermal plants were simply switched off to mimic their decommissioning as RESs take over. The Power to Gas (P2G) technology was considered as a repowering of some of the old thermal plants and located accordingly, biogas (bioenergy) and waste-to-energy technologies were modelled assuming they are brown field.

Table 3. Current RES installed in Sicily (beginning of 2020) [39].

Technology	Total Installed (MW)	MV Connected (%)	HV Connected (%)
Photovoltaic	1422	97.00	3.00
Wind	1887	6.00	94.00
Hydro	274	4.00	96.00

In the following, the major changes applied to the 2020 grid to meet the 2050 data of Task 1.2, showed in Table 4, are described.

1. Power rating of the cables with the mainland were increased to 2300 MW to meet the Available Transfer Capacity (ATC) data provided.
2. An equivalent synchronous machine was installed close to the continental terminal of the link Sicily-continental Italy to mimic the dynamic behavior of the rest of the Italian system. Its rated power equals the sum of the active power of the synchronous machines of the other Italian market zones at the time frame considered, divided by a power factor (0.8), and starting time constant equal to 10 s. This approach is conservative in the sense that the equivalent machine represents only a portion of the generating units of continental Italy able to provide primary frequency control. This machine is equipped with a governor, an automatic voltage regulator, and a power system stabilizer properly tuned.
3. 15 Full-Converter Wind Turbines (FCWTs) and 20 Doubly-Fed Induction Generators wind turbines (DFIG) were equipped with a controller able to provide SI (detailed in Section 2.3).

4. Already existing HV PV plants ere modelled according to [40], including its LV/MV transformer. The same PV model was installed at the MV busbars of the 285 primary substations to mimic the contribution of the dispersed generation connected to the distribution grids. All PV models are equipped with the overfrequency protections, set according to the Italian standards [38,41].
5. A BESS model able to provide FFR (detailed in Section 2.4) was considered. BESSs are installed either near each new wind plant or at the sites of the few synchronous generators not decommissioned. The total amount of storage power was installed according to Task 1.1. These BESS were sized equal to the 20% of the capacity of the already installed generation plant.
6. Controlled loads able to provide both SI and FFR (detailed in Section 2.5) were installed near 16 already existing loads considered large enough (at least 13 MW in the Terna base model).
7. The 230 kV ring circuit of the Island was doubled, even if no indications regarding the zonal grid reinforcements are given by the other Tasks. This solution was carried out to accommodate the demand expected for 2050.
8. Capacities of all generators were upgraded according to the data provided by Task 1.1 (Table 4). Table 5 shows the ratings and the location of the remaining synchronous machines and their identification names.

Table 4. Installed capacity (MW) provided by Task 1.1 for 2050 for Sicily [25].

Zone	Battery	PV	Hydro	Wind	Waste	Gas	P2G
56IT	1572	6075	313	6360	566	162	1947

Table 5. Ratings and location of the synchronous power plants in 2050.

Location	Identification Name	Rating (MVA)
Contrasto	CNTP	24
Dittaino	DITP	23
Priolo Gargallo	EGNP	576
Città Giardino	EGSP	90
Augusta	ESSP	80
Priolo Gargallo	ISBP	344
Paternò	PATP	9
Priolo Gargallo	PRGP	658
Milazzo	TEMP	185
Termini Imerese	TIMP	946
Troina	TROP	14

2.1.2. Typical Generation and Demand Conditions—Dispatching Profiles

In this analysis, only the scenario "Current Goal Achievement" (GCA) is considered. Capacities of the GCA scenario are implemented for 2050 related to the generators, while the following most typical and critical generation/demand conditions were tested, with reference to Sicily:

- Very low load/very low rotating generation in operation;
- High load/low rotating generation in operation;
- Maximum export/import of areas;
- Operational conditions with a weak network (lines out of service);
- Islanding conditions.

These snapshots were selected to represent the weaker grid conditions. They were identified by analyzing the load demand and the balance between the traditional generation and the renewable one.

From Task 1.2, the level of generation, differentiated by the primary sources, the active power demand, and the import (or export) in MW for each hour of one entire

year are available. The profiles provided were carefully analyzed, and, to achieve the aforementioned critical conditions, the most appropriated hours, considered to better resemble the desired situations, were picked up. Reactive power was not taken into account by Task 1.2. To keep a realistic load behavior, typical values of power factor, based on the characteristics of the Italian power system, were assigned to the loads of the Sicilian zone. Finally, the active load demand was adjusted using a suitable scaling factor to increase, or decrease, the total demand and achieve the desired values.

The following dispatching profiles (DPs), derived from the data provided by RTE, were picked up and implemented for the 2050 Sicilian grid:

- *High Export*: represented by 24th of May of MC 4 at 2:00 a.m., characterized by quite high wind production, no photovoltaic, and low load demand.
- *High Import*: represented by 11th of January of MC 1 at 1:00 a.m., characterized by almost no renewable production and medium/high demand.
- *High Load*: represented by 27th of May of MC 1 at 4:00 p.m., characterized by high load demand, high wind, and photovoltaic production.
- *Island*: represented by the 23rd of June of MC 5 at 3:00 p.m.; with high photovoltaic and wind production and the link with the mainland out of service.
- *Low Load*: represented by the 4th of June of MC2 at 2:00 a.m., characterized by low load and almost zero wind production.
- *Lines out of service*: it is the *Low Load* profile with the Favara/Chiaramonte and Caracoli/Sorgente 230 kV lines out of service.

A detailed description of these six DPs is reported in Table 6. Table 7 reports the operating points of the 16 controlled loads in any of the dispatching profiles introduced.

Table 6. Hourly dispatching profiles (MW) [27,29].

Dispatching Profile	High Export	High Import	High Load	Island	Low Load	Lines Out of Service
Time	24 May 2050 02:00	11 January 2050 01:00	27 May 2050 16:00	23 June 2030 15:00	4 June 2050 02:00	4 June 2050 02:00
MC Year	4	1	1	5	2	2
Zonal export (MW)	725	−1188	0	0	−578	−578
Loads						
Total Load (MW)	1837	3218	4099	4294	1514	1514
Traditional load (MW)	1837	3218	2318	2500	1514	1514
DSR Electrical Vehicle (MW)	0	0	0	0	0	0
Pumping (MW)	0	0	0	0	0	0
Electrolyser (MW)	0	0	1781	1794	0	0
Battery Storage (MW)	0	0	0	0	0	0
DSR Heat Pump (MW)	0	0	0	0	0	0
Generation						
Total Generation (MW)	2562	2030	4099	4294	936	936
ROR (MW)	30	11	30	25	25	25
WIND (MW)	1480	253	2059	1124	195	195
SOLAR (MW)	0	0	1211	2429	0	0
NUCLEAR (MW)	0	0	0	0	0	0
COAL (MW)	0	0	0	0	0	0
GAS (MW)	0	0	0	0	0	0
BATTERY (MW)	786	0	0	0	0	0

Table 6. *Cont.*

Dispatching Profile	High Export	High Import	High Load	Island	Low Load	Lines Out of Service
Generation						
PSP (MW)	0	0	0	0	0	0
P2G (MW)	0	1500	533	450	450	450
CHP (MW)	0	0	0	0	0	0
BIOENERGY (MW)	266	266	266	266	266	266
H. STOR (MW)	0	0	0	0	0	0
SPIL. ENRG (MW)	0	0	0	0	0	0
UNSP. ENRG (MW)	0	0	0	0	0	0
Continental Italy Equivalent Generator						
NOMINAL POWER (MVA)	10,411	1493	23,053	9607	13,533	13,533

Table 7. Loads associated with the DSR models.

	Active Power (MW)					
Load	**High Export**	**High Import**	**High Load**	**Island**	**Low Load**	**Lines Out of Service**
Load 1	42.8	42.8	59.92	59.92	21.4	21.4
Load 2	13.8	27.6	38.64	38.64	13.8	13.8
Load 3	14.5	29	40.6	40.6	14.5	14.5
Load 4	13.9	27.8	38.92	38.92	13.9	13.9
Load 5	13.3	26.6	37.24	37.24	13.3	13.3
Load 6	15	30	42	42	15	15
Load 7	126.6	189.9	177.24	177.24	0	0
Load 8	13.5	27	37.8	37.8	13.5	13.5
Load 9	16.9	33.8	47.32	47.32	16.9	16.9
Load 10	15	30	42	42	15	15
Load 11	13.4	26.8	37.52	37.52	13.4	13.4
Load 12	52.4	52.4	73.36	73.36	26.2	26.2
Load 13	13.8	27.6	38.64	38.64	13.8	13.8
Load 14	13.6	27.2	38.08	38.08	13.6	13.6
Load 15	14.8	29.6	41.44	41.44	14.8	14.8
Load 16	13.3	26.6	37.24	37.24	13.3	13.3
TOTALS	**406.6**	**654.7**	**827.96**	**827.96**	**232.4**	**232.4**

In the following, we provide a detailed description of models of wind generators, BESSs, and flexible loads, which are all able to provide frequency and/or voltage regulation services. This description is of particular interest since the main question of the present study is if the 2050 European power system will be stable and how much flexibility services from RES, BESSs, and DSR would be necessary.

2.2. Wind Generators Models

2.2.1. Full-Converter with Synthetic Inertia

SI corresponds to the controlled action of an inverter-based generating unit to mimic the kinetic energy exchanged by a synchronous generator with the power system. Different mechanisms are available in the literature to relate the frequency variation with the converter injection; here, the emulation is obtained by acting on the control of a back-to-back converter [42]. Basically, this strategy emulates the inertial response supplying a temporary contribution during the first instants of a frequency transient, exploiting the energy content of the capacitor of the DC-link [6,7], suitable oversized, thanks to the use of supercapacitors, or "ultra-capacitors".

This control model was implemented (referred as the *current-controlled* model) and tested in the wind turbine model shown in Figure 2a. This SI control could be applied to whatever type of plant connected with a fully rated converter, introducing a sufficient energy buffer.

Figure 2b depicts the adopted control diagram (a typical synchronous-frame structure is considered), where:

- Two linear Proportional-Integral (PI) regulators (suitably equipped with saturation) are introduced. These two independent controllers are associated with the DC bus stabilization and reactive injection. They provide the direct i_d^{ref} and quadrature i_q^{ref} references for the internal current loop.
- An additional signal p_{in}, introduced on the direct-axis reference and proportional (by the inertia coefficient K_{in}) to the frequency approximate derivative, enables the inertial control. Its negative sign is introduced to increase active power injection in case of underfrequency events, exploiting the discharge of the DC capacitor. Indeed, the DC voltage can temporarily vary in response to the system frequency disturbance and allow the inertial response of the converter.

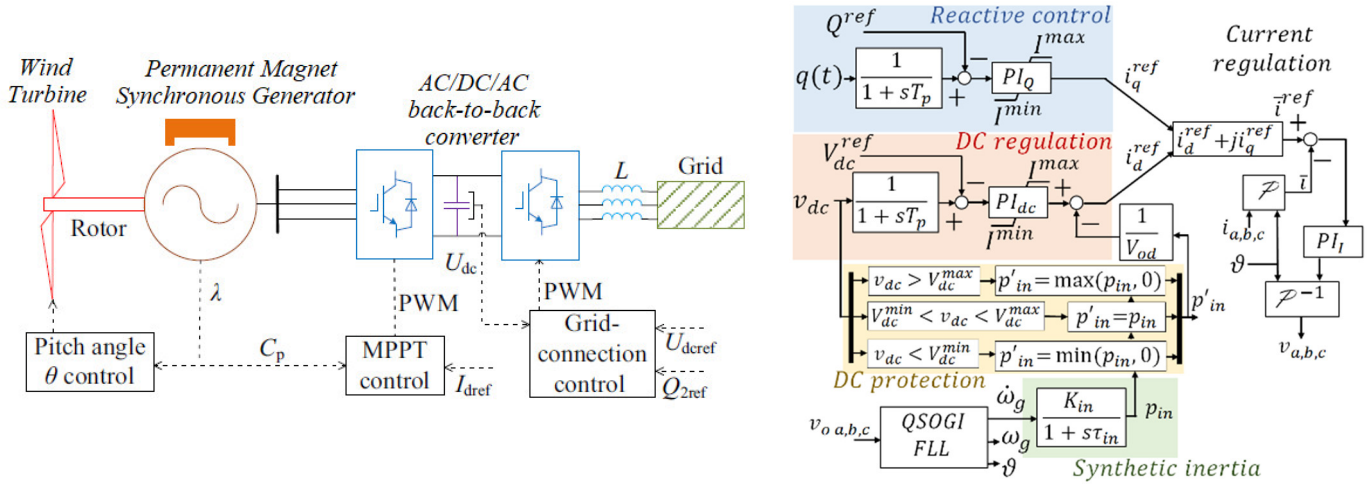

Figure 2. Full-converted wind turbine model [43] (**a**), and current controlled model for SI [6,7] (**b**).

In order to extract the angular frequency derivative $\dot{\omega}_g$, the QSOGI-FLL (Quadrature Second-Order Generalized Integrator—Frequency Locked Loop) algorithm is adopted [44]. The QSOGI-FLL system is also exploited to determine the synchronization angle for the Park transform (the capital *P* in Figure 2b). An additional filtering effect has also been introduced, combining the FLL dynamics with a first-order low-pass (with a time-constant τ_{in}):

$$p_{in} = \frac{K_{in}}{1 + s\,\tau_{in}}\,\dot{\omega}_g \tag{1}$$

Assuming a variability range $\Delta\dot{V}_{dc} = 0.1$ p.u., the sizing of the capacitor is given by:

$$C_{DC} = \frac{10\%\ A_b\ \Delta t}{\frac{1}{2}\left(V_{dc}^{nom2} - V_{dc}^{min2}\right)} \tag{2}$$

where:

- A_b is the nominal power of the equivalent wind generator exploited;
- Δt is the maximum time-length of the frequency transient supported;
- V_{dc}^{nom} is the nominal DC voltage;
- V_{dc}^{min} is the minimum allowed DC voltage.

The "DC protection" was introduced to decouple the design of the inertia coefficient K_{in} from the grid dynamics. This block guarantees the maximum exploitability of the available energy reserve and fulfills the technical/security constraints associated with the converters. Indeed, SI control is active only when the discharge process is compatible with the DC voltage ratings, in particular:

- When DC voltage is lower than the minimum allowed value (V_{dc}^{min}), discharge is inhibited, and only charging operations are allowed;
- Discharging signals can be sent to the control whenever the voltage is close to its maximum and charging operations are inhibited.

This logic can be identified in Figure 2b.

2.2.2. DFIG with Synthetic Inertia

For the DFIG wind models turbines considered, as shown in Figure 3, a different architecture to realize the DC-link SI known as the voltage-controlled model was adopted.

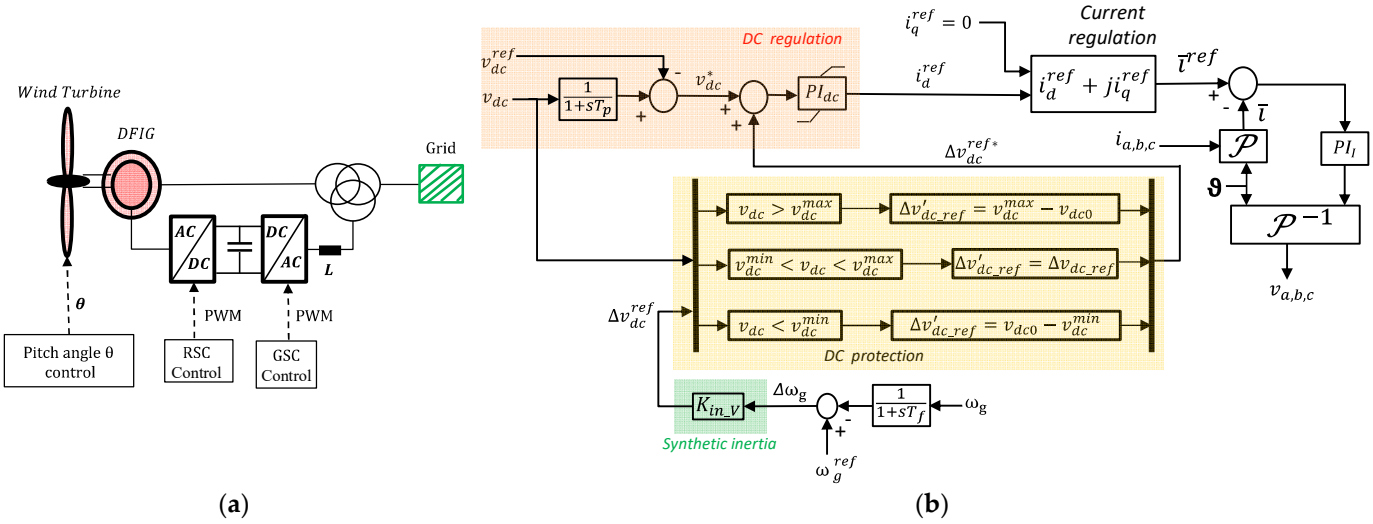

Figure 3. DFIG model [45] (**a**), and voltage controlled model for SI [4,46,47] (**b**).

Figure 3b depicts the control scheme, which considers a proportional relation between the DC-link voltage reference and the measured network frequency deviation. A frequency controller with a constant gain K_{in_V} takes the frequency deviation signal as the input and the variation of the DC voltage reference as output.

The dynamics of the DC-link voltage controller is made very fast to allow the stored electrostatic energy to be released/absorbed in response to the DC-link voltage deviation and allow SI provision. The scheme links frequency and DC-link voltage in such a way that: (i) the change in network frequency will lead to a change in DC-link voltage and (ii) the derivative of the resulting change in DC-link voltage causes the absorption or release of power from DC-link capacitors [4]. By setting the q-axis reference rotor current to zero, the reactive power flow from the Grid Side Converter (GSC) is regulated to zero to reduce the GSC rating.

The Voltage Control Mode DC protection scheme, although a bit different from the Current Control Mode SI DC protection scheme (they both have similar objectives of keeping the DC voltage within v_{dc}^{max} and v_{dc}^{min}) takes the output of the SI scheme and measured DC voltage as the input and limits the inertial response outputs to values compatible with the DC voltage ratings.

2.3. Battery Energy Storage Systems Model

BESSs were implemented using the library model available in DIgSILENT PowerFactory [31]. As shown in Figure 4, the battery is represented as an equivalent DC voltage

generator whose voltage U_{DC} depends on the battery State of Charge SoC. Current I_{DC} exchanged by the battery is driven by a Pulse-Width Modulation (PWM) AC/DC converter. I_{DC} depends on the direct and quadrature AC currents I_d and I_q, which are imposed by the PWM converter, according to the reference signals I_d^{ref} and I_q^{ref}, in turn defined by the "PQ controller". The latter implements PI regulators to realize the exchange of active and reactive powers, P^{ref} and Q^{ref}, required by the user.

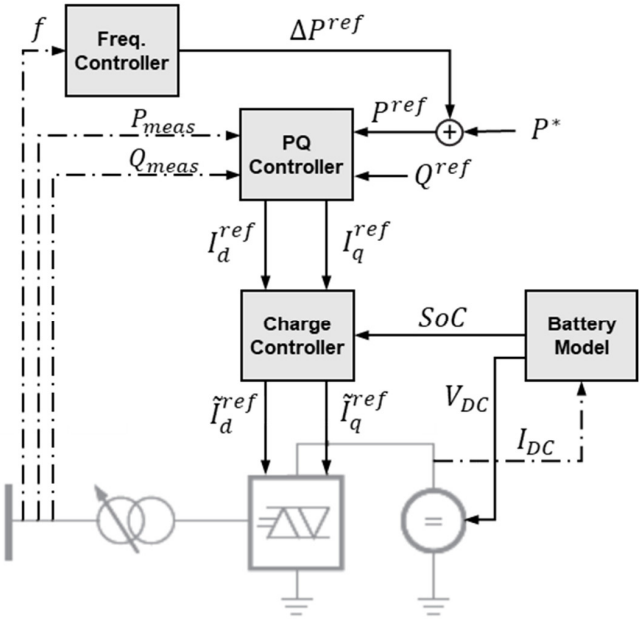

Figure 4. BESS model available from DIgSILENT PowerFactory [31].

As shown in Figure 4, P^{ref} is the sum of the set-point P^* and the variation ΔP^{ref} defined by the "Frequency Controller" to realize the FFR service. The scheme in Figure 5 shows that the FFR is realized by a simple droop controller with a dead-band set to 0.01 Hz and the droop coefficient b.

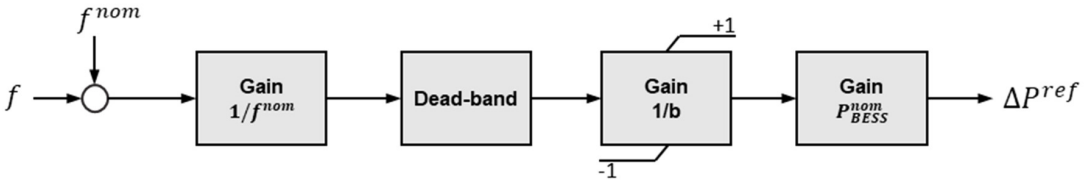

Figure 5. Frequency Controller model.

The "Charge Controller" block limits the current import, when the battery is fully charged ($SoC = 1$), and the current export, when the battery is fully discharged ($SoC = 0$).

The battery SoC is determined by a simple Coulomb counting model:

$$SoC(t) = -\frac{1}{C_b \cdot 3600} \int_0^t I_{DC}(\tau) d\tau + SoC_0, \quad (3)$$

where C_b is the battery capacity in Ah and SoC_0 is the initial condition. Two important assumptions worth to be mentioned are that capacity C_b is constant, and voltage U_{DC} is linearly dependent on the SoC. These approximations are acceptable in the context of the present study since dynamical simulations are executed in a time scale from tens of milliseconds up to tens of seconds.

Within the DIgSILENT model, capacity C_b is determined as $C_b = N_c^{par} \cdot C_c$, where N_c^{par} is the number of parallel cells and C_c is the capacity of the single cell. The nominal DC voltage is determined as $U_{DC}^{nom} = N_c^{ser} \cdot u_{max}$, where N_c^{ser} is the number of series cells

and u_{max} is the voltage of full cells. Moreover, the DIgSILENT model allows setting the BESS rated power P_{BESS}^{nom}. All implemented BESSs adopt the parameters reported in Table 8, whereas N_c^{par} is defined to obtain a desired capacity C_{BESS} in Wh such that $P_{BESS}^{nom} = C_{BESS}/1$ h.

Table 8. BESS common parameters [1].

Parameter	Symbol	Value
Single cell capacity	C_c	50 Ah
Voltage of full cells	u_{max}	15 V
Voltage of empty cells	u_{min}	12 V
Number of series cells	N_c^{ser}	60
Battery nominal voltage	U_{DC}^{nom}	0.9 kV
Converter AC side nominal voltage	U_{AC}^{nom}	0.4 kV
Cells internal resistance	Z_i	0.001 Ω

[1] For details of parameters not introduced in the text, the reader is referred to [31].

2.4. DSR

By suitably modulating their power consumption, electrical loads equipped with a form of energy storage (e.g., thermal energy in thermal loads) can provide frequency regulation services to the power system. Scientific literature has proposed many solutions in order to allow commercial buildings [11], industrial compounds and/or aggregates of domestic loads [9,10] to provide frequency regulation services. In general, even if with different levels of robustness, depending on the proposed control architecture and on the typology of loads, in all these works, loads are made able to follow a reference signal designed to provide SI and FFR.

Ideally, the reference signal is

$$\Delta P_L^{ref}(t) = K_{FFR}\Delta f(t) + K_{SI}Df(t), \tag{4}$$

where: $\Delta f(t)$ is the frequency deviation at time t, Df is the frequency derivative at time t (RoCoF); K_{FFR} is the FFR coefficient, and K_{SI} is the SI coefficient. The values of these two last coefficients depend on the type of loads and on the adopted control strategy. K_{FFR} is an equivalent droop coefficient, whereas K_{SI} is the provided amount of SI.

In any case, the reference signal ΔP_L^{ref} cannot be perfectly followed, mainly due to the fact that the input values of the controller are not the real-time values of frequency deviation Δf and frequency derivative Df, but the measured values Δf^m and Df^m, collected with a certain sampling time and then filtered with a low-pass filter, as shown in Figure 6 (according to the ENTSO-E "Demand Connection Code" [48]).

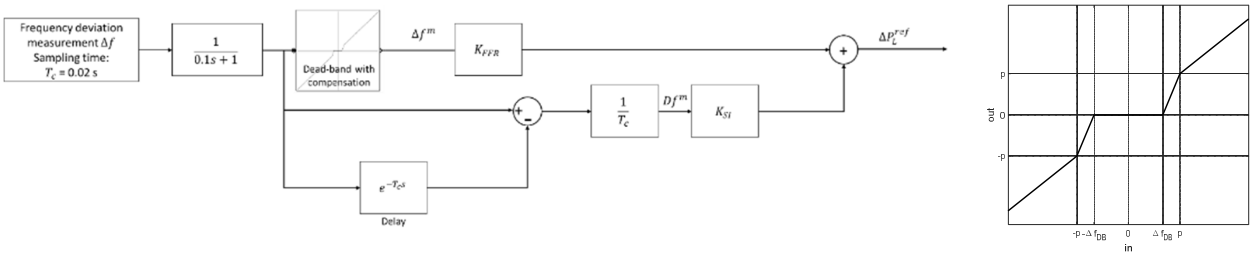

Figure 6. Measurement chain for frequency and RoCoF (**left**). Detail of the dead-band with compensation (**right**).

Therefore, (4) is substituted by:

$$\Delta P_L^{ref}(t) = K_{FFR}\Delta f^m(t) + K_{SI}Df^m(t), \tag{5}$$

where $\Delta f^m(t)$ and $Df^m(t)$ are the measured values of the two mentioned quantities. The dead-band is defined by two parameters: Δf_{DB}, which determines the band amplitude and the break point p. In all simulations, $\Delta f_{DB} = 0.02$ Hz and $p = 0.03$ Hz.

The value of K_{FFR} should be defined in function of the FCR, in [37] is defined as the *active power reserves available to contain system frequency after the occurrence of an imbalance*. According to [37], each TSO must secure that the combined reaction of FCR respects with the following requirements:

A. FCR is not artificially delayed and begins as soon as possible after a frequency deviation;
B. If the frequency deviation is equal to or larger than 200 mHz, at least 50% of the full FCR capacity must be delivered at the latest after 15 s; and 100% of the full FCR capacity must be delivered at the latest after 30 s. Moreover, the activation of the full FCR capacity must rise at least linearly from 15 to 30 s;
C. If the frequency deviation is smaller than 200 mHz, the activated FCR capacity must be at least proportional with the same time behavior referred in points (A) and (B).

2.5. Methodology

The methodology adopted in this study, detailed in the following sections, is described by the flowchart depicted in Figure 7.

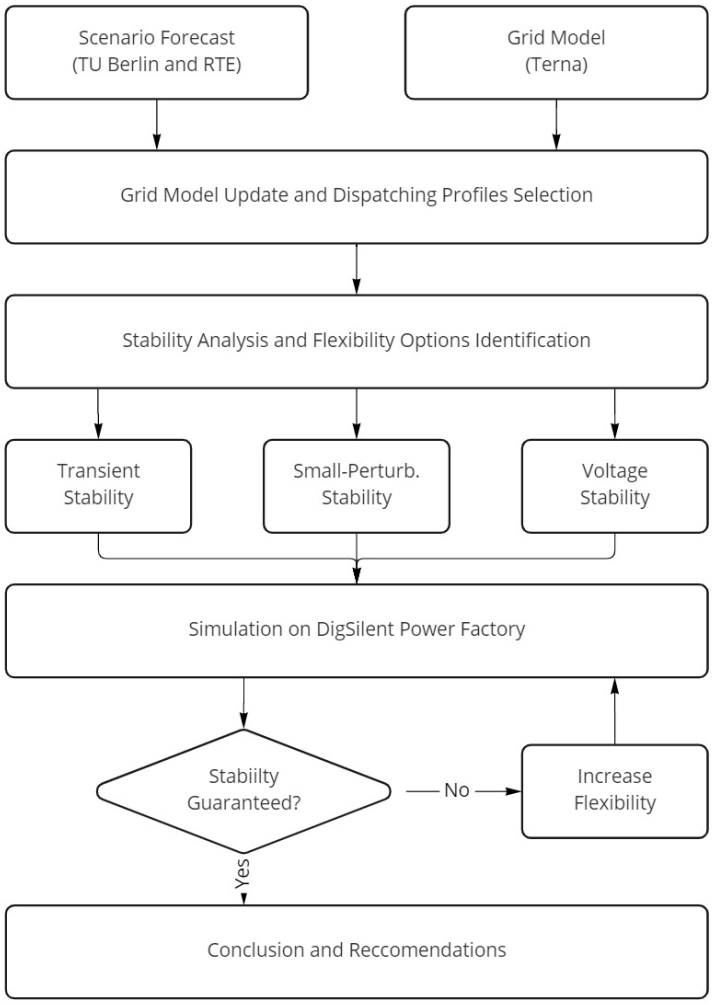

Figure 7. Stability analysis: methodology flowchart.

As shown in the figure, the grid model is updated and the DPs are selected taking as inputs the 2050 scenario forecast provided by Task 1.1 and 1.2 and the 2020 Italian grid model provided by Terna. For each DP a transient stability analysis, a small-perturbation

stability analysis and a voltage stability analysis are performed in DIgSILENT PowerFactory. If the DP does not comply with one of the stability conditions, additional flexibility tools are implemented (e.g., SI, DSR) or their contribution is increased to the extent until stability is guaranteed. Finally, the identified solutions able to provide stability even in the most critical operating conditions are examined in the conclusions and recommendations section.

3. Large Perturbation Stability Analysis

Large perturbation stability analysis is carried out by dynamical simulations on a time scale from tens of milliseconds up to tens of seconds. In particular, electromechanical stability is assessed, considering the dynamics of generators and loads and the triggering of protection schemes.

The six DPs of Table 6 are considered, and for each of them, a set of events is simulated. Specifically, the following events are simulated:

- The outage of one or two of the three connections with the mainland (except for the Island DP);
- A 500 MW load-step occurring in continental Italy (load-step in continental Italy is not considered in the Island DP);
- The outage of groups of large generating units.

3.1. Frequency Stability Definitions

According to the Italian grid code [49]:

- In Normal Operating Conditions (NOC), the frequency must remain within the range 49.9–50.1 Hz;
- For the special case of Sicily disconnected from the mainland, the NOC range is 49.5–50.5 Hz;
- In Emergency Operating Conditions (EOC), the frequency must be kept in the range 47.5–51.5 Hz.

Notice that if frequency exceeds the EOC range of 47.5 Hz or 51.5 Hz, a system blackout can hardly be avoided [50]. Therefore, for our simulations, stability is guaranteed if the numerical integration converges, and frequency is kept within 47.5–51.5 Hz. Moreover, a simulation is labelled as follows:

1. *Strongly stable*, if stability is guaranteed and frequency remains within the NOC limits;
2. *Stable*, if stability is guaranteed, but NOC are violated;
3. *Unstable*, if stability is not guaranteed.

3.2. Network Configurations

The objective of the present study is to analyze if the 2050 power system of Sicily can assure frequency stability. According to the results provided in the OSMOSE Task 1.1 [25], both BESSs operating FFR and flexible loads providing DSR will be available. Therefore, simulations are carried out with the *base configuration*, without BESS FFR and DSR, and with further network configurations with BESS FFR and/or DSR.

3.2.1. Configurations with BESS FFR

As described in Section 2.2, BESS FFR is implemented as a droop controller, essentially defined by the droop coefficient b, which states the amount of FCR provided by the BESS. Specifically, the i-th BESS with nominal power $P^{nom}_{BESS,i}$ will provide, at steady-state, the following power variation:

$$\Delta P_{BESS,i} = \frac{100}{b} \frac{\Delta f}{f^{nom}} P^{nom}_{BESS,i}. \quad (6)$$

In this analysis, the same droop coefficient is assumed for all BESSs in service with values within the interval 1–5%, and the relevant network configuration is indicated with BESS-b. It is worth noticing that 4–5% are typical droop coefficient values adopted for

traditional (hydro or thermal) generators. In this study, lower droop values are considered since BESSs could potentially be installed to exclusively provide FFR. Therefore, the droop can be lowered more than in the case of generators. In particular, since the simulated BESSs are associated with wind and traditional generators, and their nominal powers are assumed equal to the 20% of the relevant generators, a droop coefficient equal to 1% means that the BESS emulates the 5% droop frequency response of the associated generator. Obviously, a general hypothesis is that all BESSs are provided with an energy reserve sufficient to realize the regulation service, i.e., their *SoC* at the event occurrence is such that power variation in (5) can be kept up to a prescribed maximal time interval (a typical value is 15 min).

By adopting Δf_{max} = 0.2 Hz as the frequency deviation at which the full FCR should be released (according to [37]), the FCR provided by the i-th BESS is:

$$FCR_{BESS,i} = \min\left(\frac{100}{b} \cdot \frac{0.2}{f^{nom}} \cdot P^{nom}_{BESS,i}\,,\ \ P^{nom}_{BESS,i} - \left|P^{0}_{BESS,i}\right|\right), \tag{7}$$

where $P^{0}_{BESS,i}$ is the i-th BESS working point. In the following, FCR^{tot}_{BESS} will indicate the total FCR provided by all BESSs providing FFR, i.e., $FCR^{tot}_{BESS} = \sum_i FCR_{BESS,i}$.

3.2.2. Configurations with DSR

DSR is operated by the 16 loads listed in Table 7. To simplify the sizing of the DSR service, described in detail in Section 2.3, parameters FCR_{FFR} and FCR_{SI} are set equal to the same tuning value FCR_{DSR}. For the i-th load, $FCR_{DSR,i}$ is defined as a percentage p (%) of the load working point $P_{L,i}$:

$$FCR_{DSR,i} = \frac{p}{100} \cdot P_{L,i}. \tag{8}$$

Given p, the relevant network configuration will be indicated as DSR-p. Moreover, FCR^{tot}_{DSR} will indicate the total FCR and SI provided by all the 16 loads, i.e., $FCR^{tot}_{DSR} = \sum_i FCR_{DSR,i}$.

3.2.3. Simulations Procedure

For each DP and for each event, the following procedure is followed. The *base configuration* is firstly tested. Then, if strong stability cannot be guaranteed, network configurations with BESS FFR are simulated by progressively decreasing the droop coefficient from 5% to 1%. If this is not sufficient to obtain strong stability, further network configurations with both BESS FFR and DSR are tested by progressively increasing the DSR percentage parameter p up to 35%.

3.3. Results

Table 9 provides an overview of the obtained results. For each simulation, the table reports if strong and/or simple stability was guaranteed with the *base configuration*. In the cases where one of these two conditions is not satisfied, Table 9 reports the amount of FCR provided with the "best" BESSs-DSR configuration ($FCR^{tot}_{BESS} + FCR^{tot}_{DSR}$) and if, in this case, the two conditions were successfully satisfied. As best BESSs-DSR configuration, we intend the one with the lowest level of contribution from BESSs and DSR (highest droop coefficient and lowest p) allowing frequency regulation performances to be improved.

Table 9. Large perturbation stability analysis: simulation results.

Event	Base Configuration		Best BESSs—DSR Configuration			
	Stable?	Strongly Stable?	Configuration	FCR	Stable?	Strongly Stable?
High Export						
Load-step in continental Italy (500 MW)	YES	NO	BESS-1 DSR-25	655 MW	YES	YES
Outage of 1 link with continental Italy	YES	YES	Not required	-	-	-
Outage of 2 links with continental Italy	YES	YES	Not required	-	-	-
Generation outage (220 MW)	YES	YES	Not required	-	-	-
High Import						
Load-step in continental Italy (500 MW)	YES	NO	BESS-5 DSR-15	203 MW	YES	YES
Outage of 1 link with continental Italy	YES	YES	Not required	-	-	-
Outage of 2 links with continental Italy	NO	NO	BESS-1	522 MW	YES	YES
Generation outage (321 MW)	YES	YES	Not required	-	-	-
Generation outage (569 MW)	YES	NO	BESS-3 DSR-25	338 MW	YES	YES
Generation outage (817 MW)	YES	NO	BESS-1 DSR-35	751 MW	YES	NO
High Load						
Load-step in continental Italy (500 MW)	YES	YES	Not required	-	-	-
Outage of 1 link with continental Italy	YES	YES	Not required	-	-	-
Outage of 2 links with continental Italy	YES	YES	Not required	-	-	-
Generation outage (337 MW)	YES	YES	Not required	-	-	-
Island						
Generation outage (337 MW)	YES	NO	BESS-3	174 MW	YES	YES
Low Load						
Load-step in continental Italy (500 MW)	YES	NO	BESS-1 DSR-30	362 MW	YES	YES
Outage of 1 link with continental Italy	YES	YES	Not required	-	-	-
Outage of 2 links with continental Italy	YES	YES	Not required	-	-	-
Generation outage (337 MW)	YES	NO	BESS-1	292 MW	YES	YES
Lines out of service						
Load-step in continental Italy (500 MW)	YES	NO	BESS-1 DSR-30	362 MW	YES	NO
Outage of 1 link with continental Italy	YES	YES	Not required	-	-	-
Outage of 2 links with continental Italy	YES	YES	Not required	-	-	-
Generation outage (337 MW)	YES	NO	BESS-3 DSR-30	362 MW	YES	YES

As we can observe in Table 9, with the *base configuration*, frequency stability is guaranteed in all the DPs and for all events, except for the outage of two connections with continental Italy in the *High Import* DP. In this case, the loss of the two connections causes the outage of the third remaining one. This outage happens because the high level of imported power, equal to 1188 MW, leads the current on the third cable to overcome the rated value. In this condition, we assume that an overcurrent protection is installed, causing the trip of the cable and the islanding of Sicily. It is worth remarking that such a situation is unrealistic and would never occur. However, we study this case as an extreme situation to assess the potential of the flexibility available.

Figure 8 shows the frequency profile and its time derivative obtained in this specific scenario. In this figure, results obtained with the *base configuration* are not reported since they are unstable. In Figure 8a, we observe that in configuration BESS-5, with a total additive FCR of 105 MW, frequency reaches a minimum of 48.9 Hz, before starting to increase toward a steady-state value of about 49.1 Hz. This behavior is obtained thanks to the activation of two load shedding steps. Indeed, at about 2.8 s, frequency overtakes the threshold of 49.3 Hz and, as shown in the zoom in Figure 8, the frequency derivative is lower than -0.3 Hz/s. According to Table 2, this causes the shedding of 9% of loads (equal

to 290 MW). Then, always according to Table 2, when the frequency reaches the threshold of 48.9 Hz a further shedding of the 8% of loads (equal to 257 MW) is triggered.

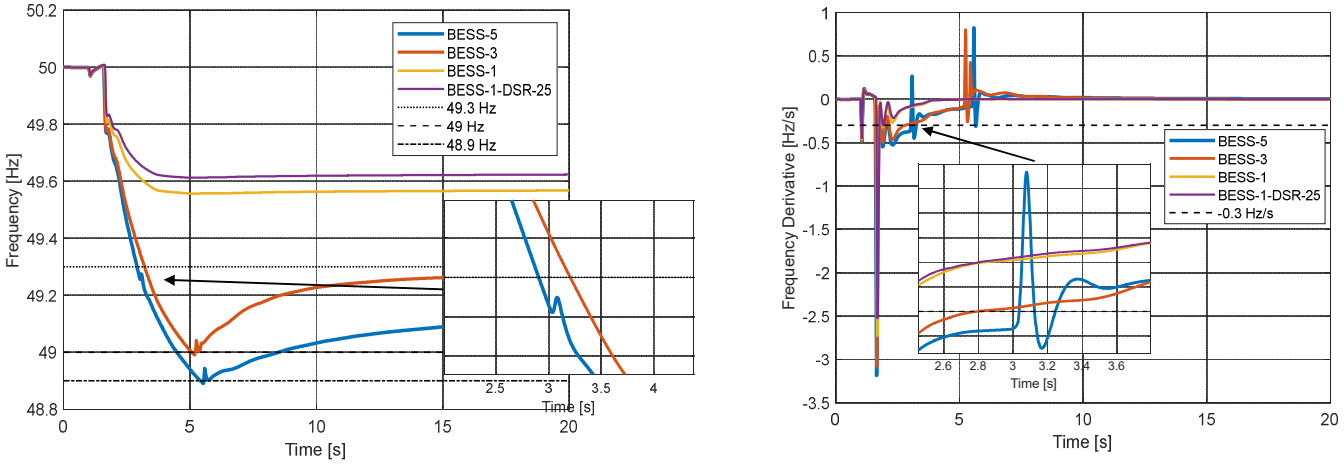

(**a**) (**b**)

Figure 8. *High Import* DP, outage of two of the three connections with continental Italy: (**a**) frequency profiles; (**b**) frequency derivative profiles.

Increasing the BESS contribution, in configuration BESS-3, with a total additive FCR of 174 MW, the shedding at 49.3 Hz is avoided since the overtaking of this threshold is delayed at about 3.2 s (as we can observe in the zoom in Figure 8a), when frequency derivative is higher than the threshold of −0.3 Hz seconds (as we can observe in the zoom in Figure 8b). However, frequency reaches the threshold of 49 Hz, causing the shedding of the 9% of loads (equal to 290 MW), according again to Table 2. Finally, the frequency reaches a steady-state value close to 49.3 Hz.

Therefore, with the support of BESSs, in the two configurations BESS-5 and BESS-3, frequency stability is guaranteed but: (i) load shedding is activated and (ii) the NOC threshold of 49.5 Hz is violated. Augmenting the BESS contribution again, with a lower droop coefficient, in the configuration BESS-1, with a total additive FCR of 522 MW, load shedding is avoided, and frequency is kept higher than the 49.5 Hz threshold. A similar result, with a lower frequency deviation, is obtained with the BESS-1 DSR-25 configuration, where BESSs and DSR provide a total additive power reserve of 684 MW.

Always observing results in Table 9, we notice that in some cases, with the *base configuration*, NOC are violated, even if stability is guaranteed. This never happens in the *High Load* DP, where the number of generating units providing FCR is sufficient to keep NOC without requiring the contribution of BESSs and DSR. Differently, in the other DPs with Sicily connected to the Italian peninsula, the 500 MW load-step occurring in continental Italy causes the violation of NOC with the *base configuration*. In these cases, the support of BESSs and DSR to frequency regulation is always sufficient to keep frequency in the range 49.9–50.1 Hz.

Further cases where the contribution of BESSs and DSR is required to keep NOC are the outages of large traditional generating units in the *High Import*, *Island*, *Low Load*, and *Lines out of service* DPs. In most cases, a suitable mix of BESSs and DSR FCR is sufficient to guarantee NOC. In only two cases, this result is not possible. The first one is the outage of a large group of generating units in the *High Import* DP, which causes the loss of 817 MW of generated power. As shown in Figure 9a, with configuration BESS-1 DSR-35, corresponding to an additive FCR of 751 MW, the violation is only 0.02 Hz for about 4 s, and the steady-state frequency value is equal to 49.9 Hz. It is clear that augmenting the DSR participation percentage again from 35% will allow not violating the threshold. For this simulation, Figure 10a shows the active power exchanged by the BESSs associated with the in-service traditional generators, FCWTs and DFIGs. Here, BESSs are exporting power when the

simulation starts. Then, when the perturbation occurs, they increase their power export to support the frequency regulation. As expected, the provided power variation is higher as lower is the droop coefficient. Figure 10b reports the variation of the active power absorbed by loads operating DSR. We can observe that, as frequency decreases, the power demand is reduced to support frequency regulation.

The second case where NOC cannot be guaranteed is the load-step in continental Italy in the *Lines out of service* DP. As shown in Figure 9b, an additive FCR of 362 MW provided by the mix BESS-1 DSR-30 is not sufficient to keep frequency higher than 49.9 Hz. In this case, we overtake the limit of $p = 35\%$ by simulating configuration BESS-1 DSR-50, corresponding to an additive FCR of 406 MW. These results are again not sufficient to keep the NOC, even if the violation of the 49.9 Hz threshold is only temporary (about 7 s) and limited to about 0.02 Hz.

It is finally worth remarking that in all simulations, all voltages levels always remain within the Italian grid code limits, and no congestion issues occur.

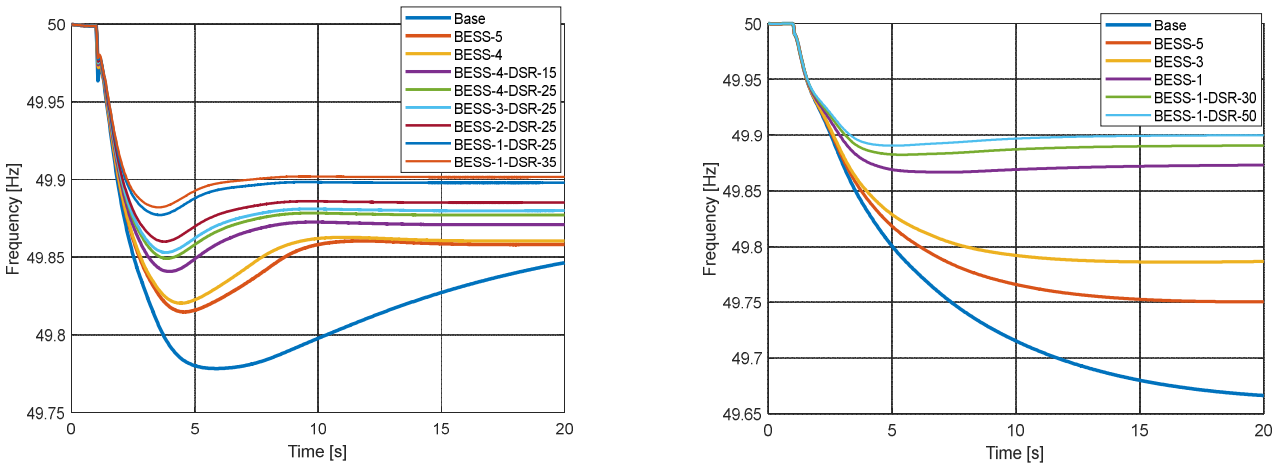

(**a**) (**b**)

Figure 9. Frequency profiles for: (**a**) *High Import* DP, generation outage of 817 MW: (**b**) *Lines out of service* DP, 500 MW load-step in continental Italy.

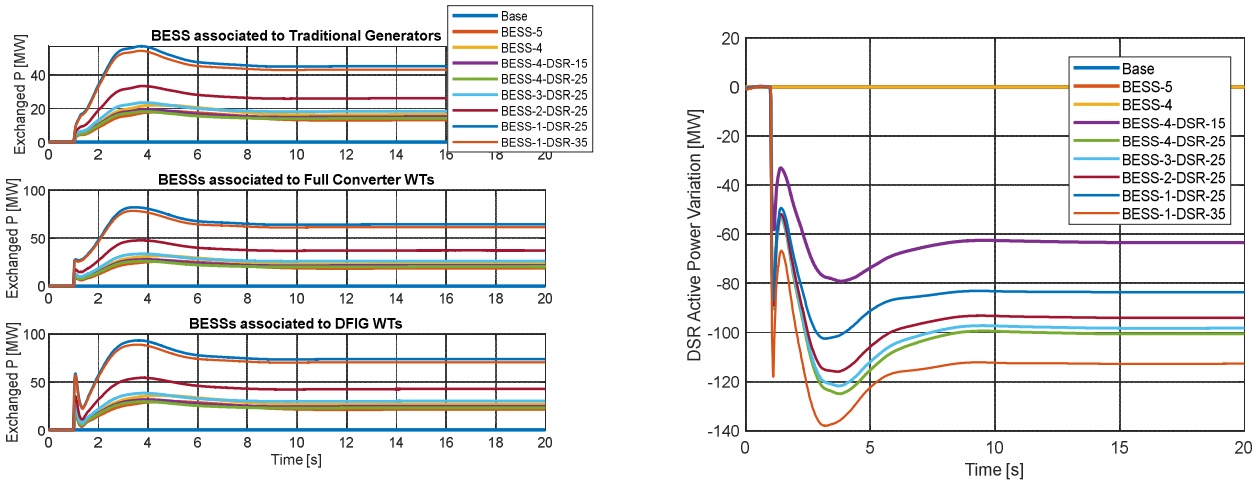

(**a**) (**b**)

Figure 10. *High Import* DP, generation outage of 817 MW: (**a**) power exchanged by BESSs (positive means export, negative means import); (**b**) total power consumption variation provided by DSR.

4. Small Signal Stability Analysis

The small perturbation stability analysis allows the evaluation of the dynamic of the generators in response to a small variation in loads and generation. Even if small signal

angle instability can be related to either the lack of synchronizing or damping torque, this instability mostly concerns insufficient damping of the system's oscillations due to large groups of closely coupled machines connected by weak tie lines [32].

4.1. Small Signal Stability Definitions

Modal analysis was performed for each of the 6 DPs presented in Table 6 to assess the small signal stability analysis of the forecasted network. A dynamic system described by state matrix A is said to be stable to small angle perturbations if, for every mode, the associated eigenvalue has a negative real part.

Damping refers to pairs of complex eigenvalues $\lambda = \sigma \pm j\omega$, which introduce oscillatory modes with a frequency equal to $f = \omega/2\pi$, and it is a measure of the rate of decay of the amplitude of the oscillations. The damping ratio is hence introduced:

$$\zeta = \frac{-\sigma}{\sqrt{\sigma^2 + \omega^2}} \tag{9}$$

which corresponds to the opposite of the real part of the eigenvalue divided by its module [51]. In the practice of electric power systems, a system is said to be stable and oscillations properly damped if the damping ratio is greater than 5%. In the following, modes with a damping ratio above 10% are not reported, and those below 5% are considered unstable; furthermore, electromechanical modes are the primary focus.

For our analysis, the *oscillation vector*, composed of the magnitude of the participation vector and the angle of the observability [52] can be used to easily identify the electromechanical modes. Indeed, the oscillation vectors allow identifying the state variables mainly involved in that mode and, by looking at the angle differences, understanding how the oscillations are manifested in the state variables, e.g., if in phase or counter-phase. In formulas, the oscillation vector of the state variable x_i with respect to mode k is:

$$ov_{ki} = |pf_{ki}| \angle w_k(i) \tag{10}$$

where pf_{ki} is the participation factor of the state variable x_i in the kth mode and $w_k(i)$ is the ith element of observability vector k (i.e., the right eigenvector associated with the mode k). This feature will be used to identify the properties specific to each relevant electromechanical mode and the behavior of the involved generators. Electromechanical modes can be generally classified into three categories depending on the location of the generators involved. In order of increasing frequency, inter-area modes involve generators belonging to distinctly different areas of the grid (e.g., Sicily and the peninsula), inter-plant or local modes are modes involving units of the same area, but different plants, intra-plant modes are modes involving units of the same plant [32].

4.2. Network Configurations

In the following sections, the small signal stability of the network in its *base configuration*, without any support provided by RES, is evaluated. Then the contribution of the SI provided by FCWT is considered, and, lastly, the gain of the PSS of the relevant generators are tuned to increase the overall stability of the grid, in particular, the damping ratio of inter-area mode called M1. Finally, the effect of the two combined actions is presented. The frequency support provided by the BESSs and DFIGs has also been investigated. For the sake of brevity, they are not presented as they provide just a minor contribution.

In Figure 11 the 12 substations' locations and denomination of the conventional plants reported in Section 2, Table 5, are shown. Each plant can have one or more units. In the following discussion, we will be referring to these units with the denomination of the plant (Identification names in Table 5) followed by a sequential number if needed. Of the 24 synchronous generators in the network, just those with a rated power equal to 70 MVA or greater, i.e., 15 of them, are equipped with a PSS. The latter provides a further input signal

to the exciter system to provide additional damping to the electromechanical oscillations of the power system through exciter control.

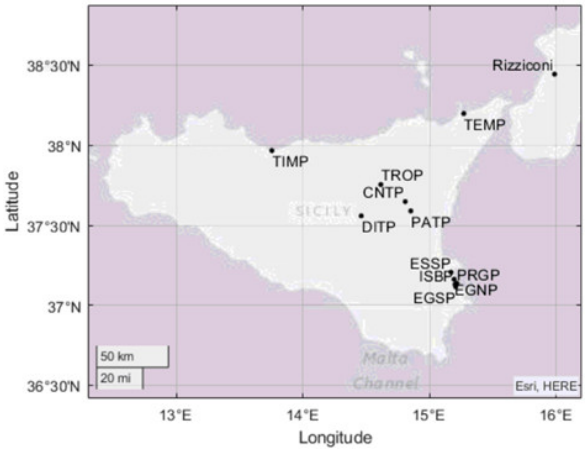

Figure 11. Locations and denominations of the traditional power plants in the Sicilian network.

4.2.1. Base Configuration

The *High Export*, *High Load*, and *Island* DPs do not present any mode with a damping ratio below 10% and are thus considered stable. The following focuses on those DPs that do present some modes with a damping ratio below 10% that is, the *High Import*, *Low Load*, and *Lines out of Service* DPs.

In the *High Import* DP, the modal analysis revealed twenty oscillatory modes with a damping ratio below 10% and all of them with a damping ratio above 5%, thus stable. Fifteen of these (modes D1 to D15) concern the DFIG units and are all very similar. For this reason, just mode D1 is discussed. The results are reported in Table 10.

Table 10. Electromechanical modes below the threshold of 10% for the *High Import* DP.

Mode	Eigenvalues	Frequency (Hz)	Damping (%)	Involved Plants
M1	-0.27 ± 4.81j	0.77	5.66	TIMP, PRGP, SLACK
D1	-0.67 ± 11.29j	1.80	5.90	DFIGs in ANPP
M2	-0.59 ± 8.18j	1.30	7.24	EGSP, PRGP
M3	-0.88 ± 9.98j	1.59	8.83	EGSP
M4	-0.89 ± 9.97j	1.59	8.90	EGSP
M5	-1.04 ± 10.44j	1.66	9.91	DITP, ESSP, PRGP

As anticipated, inspecting the oscillation vectors of the modes allows us to identify the generators involved and whether the rotors swing in phase or counter-phase.

Mode M1 has a frequency of 0.77 Hz and a damping factor of 5.66%. In Figure 12a, the oscillation vector is shown. The generators mainly affected by this oscillatory mode are generators TIMP1 and TIMP2 of the thermoelectric plant in Termini Imerese (TIMP). The mode is an inter-area mode, as the frequency suggests, in which the slack generator in Rizziconi oscillates against TIMP1, TIMP2 and generator PRGP1 in Priolo Gargallo (PRGP). The participation factors of PRGP1 and the slack are significantly lower than those of the TIMP units.

Mode M2 has a frequency of 1.30 Hz and a damping factor of 7.24%. In Figure 12b, the oscillation vector is shown. This is a local mode in which the three generators of the Erg Plant, EGSP1, EGSP2, and EGSP3 oscillate against the units in Priolo Gargallo, PRGP1, and PRGP2.

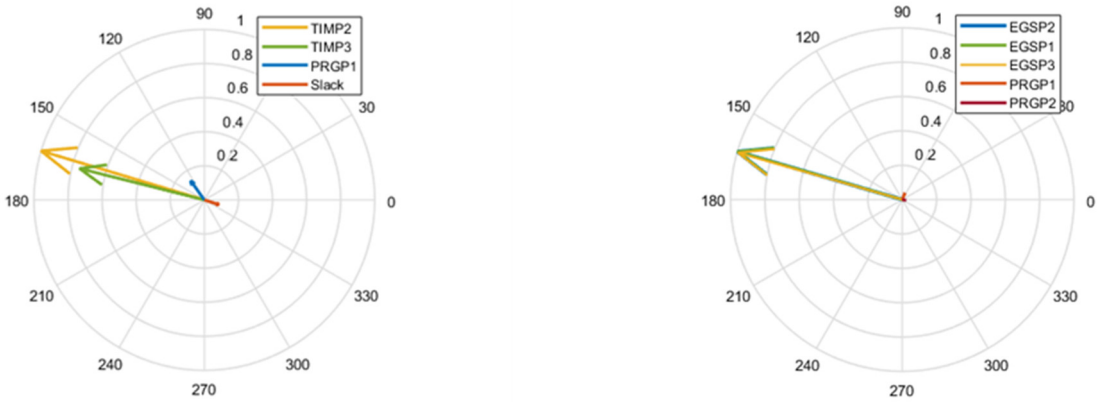

(**a**) (**b**)

Figure 12. *High Import* DP: (**a**) oscillation vector of mode M1; (**b**) oscillation vector of mode M2.

Modes M3 and M4 are both intra-plant modes concerning the units of EGSP with the same frequency, 1.59 Hz, and a damping factor of 8.83% and 8.90%, respectively. Their oscillation vectors are shown in Figure 13a,b, respectively. In mode M3, EGSP3 oscillates against EGSP1 and EGSP2, while in mode M4, EGSP1 oscillates against EGSP2 and EGSP3.

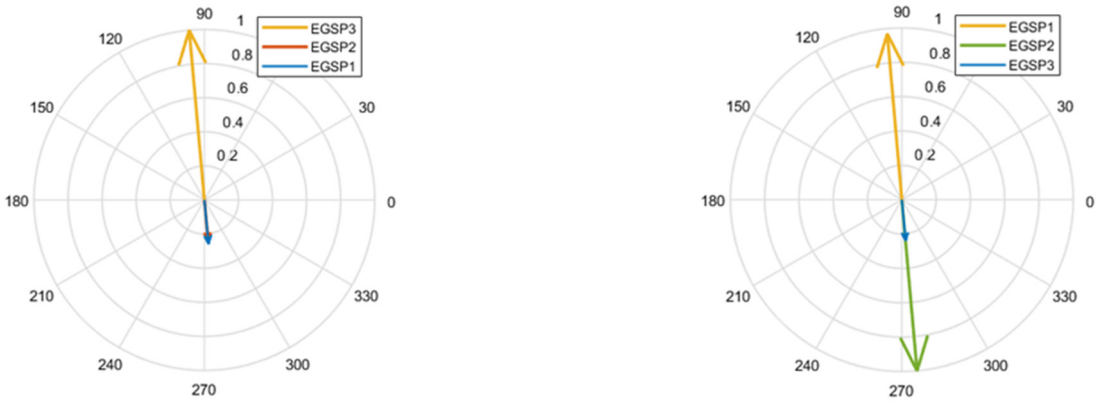

(**a**) (**b**)

Figure 13. *High Import* DP: (**a**) oscillation vector of mode M3; (**b**) oscillation vector of mode M4.

Mode M5 has a frequency of 1.66 Hz and a damping factor of 9.91%. The oscillation vector is shown in Figure 14a. This mode is a local mode in which the 22.8 MVA generator in Dittaino (DITP) and the 58.1 MVA generator in Augusta (ESSP2), both not equipped with PSS, oscillate against the larger generator located in Priolo Gargallo, PRGP1, with a rated power of 370 MVA, a large constant of inertia of 7.5 s and equipped with PSS. For this reason, the magnitude of the oscillation vector of PRGP1 effectively appears like a dot in the origin.

Mode D1, with a frequency of 1.80 Hz and a damping factor of 5.90%, involves two DFIG units located in the substation of Anapo (ANPP). In total, there are 15 modes like this one, and they involve the 15 DFIGs in the network. Since all these modes behave very similarly, for the sake of conciseness, just the first one is shown in Figure 14b. This mode is a local mode in which the rotor speed of the DFIG unit ANPP2 oscillates against the DFIG unit ANPP3.

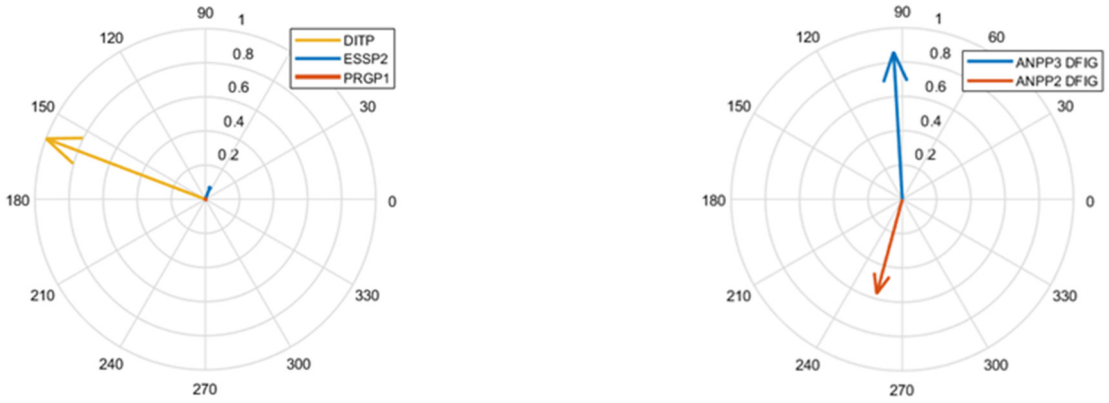

(**a**) (**b**)

Figure 14. *High Import* DP: (**a**) oscillation vector of mode M5; (**b**) oscillation vector of mode D1.

To analyze the characteristics of these 15 modes, four different wind turbine power setpoints, i.e., P = [0, 0.1, 0.2, 0.3] MW, are considered. The effects on mode D1 are presented in Table 11. While the frequency of D1 does not appear to be linked with the active power setpoint, the damping ratio of D1 is somehow correlated with the power produced. Its damping is always above the stability threshold of 5% and increases above the conservative threshold of 10% for an active power set point greater than 0.1 MW, that is, around 7% of the turbine rated power.

Table 11. Effect of the DFIG active power production on mode D1. Check marks indicate those modes with a damping factor greater than 10%.

DFIG Active Power Setpoint (MW)	Frequency (Hz)	Damping (%)
0	1.80	6.1
0.1	1.80	5.9
0.2	✓	✓
0.3	✓	✓

In the *Low Load* DP, the modal analysis revealed three electromechanical modes with a damping ratio below 10%, the inter-area mode M1, with a value of 3.88%, thus unstable. The results are reported in Table 12. As shown, the inter-area mode can be properly damped, either with the contribution of SI provided by RES (contribution of both FCWTs and BESSs), by tuning the gain of the relevant PSS or by a combination of both.

Table 12. Electromechanical modes below the threshold of 10% for the *Low Load* DP.

Mode	Eigenvalues	Frequency (Hz)	Damping (%)	Involved Plants
M1	-0.19 ± 4.95j	0.79	3.88	TIMP, PRGP, SLACK
M6	-0.80 ± 10.86j	1.73	7.38	CNTP, PRGP
M7	-0.85 ± 11.09j	1.77	7.67	PATP, CNTP

Mode M6 has a frequency of 1.73 Hz and a damping factor of 7.38%, and in Figure 15a the oscillation vector is shown. In this mode, the relatively small generator in Contrasto (CNTP, 24 MVA) oscillates against the larger unit in Priolo Gargallo (PRGP1, 370 MVA), which, being also equipped with a PSS, is practically unaffected by the oscillations. For this reason, its oscillation vector in the graph appears like a dot in the origin.

Mode M7 has a frequency of 1.77 Hz and a damping factor of 7.67%, in Figure 15b, the oscillation vector is shown. This mode involves the 9 MVA unit in Patternò (PATP) oscillating against the 24 MVA unit in Contrasto (CNTP), both not equipped with PSS.

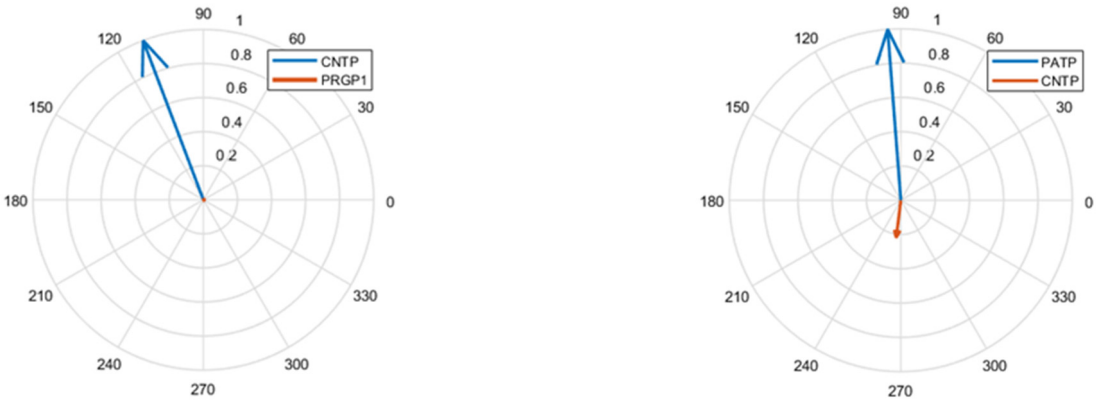

Figure 15. *Low Load* DP: (**a**) oscillation vector of mode M6; (**b**) oscillation vector of mode M7.

The *Lines out of Service* DP being a variation of the *Low Load* one, in which two important 230 kV lines (lines Favara-Chiaramonte and Caracoli-Sorgente) are out of service, presents the same three modes. The results are reported in Table 13. Mode M1 is particularly affected because the line Caracoli-Sorgente effectively connects the plant in Termini Imerese (TIMP) to the interconnection with continental Italy, right before the substation of Rizziconi.

Table 13. Electromechanical modes below the threshold of 10% for the *Lines out of Service* DP.

Mode	Eigenvalues	Frequency (Hz)	Damping (%)	Involved Plants
M1	-0.05 ± 4.73j	0.75	1.08	TIMP, PRGP, SLACK
M6	-0.86 ± 10.82j	1.72	7.95	CNTP, PRGP
M7	-0.92 ± 11.05j	1.76	8.26	PATP, CNTP

The damping ratio of mode M1 decreases from 5.66% in the *High Import* DP, to 3.88% in the *Low Load* DP, and finally to a value of 1.08% in the *Lines out of Service* DP. In the following, a combination of SI support schemes and PSS tuning are adopted to properly damp the critical inter-area mode of the network.

4.2.2. Configuration with FCWT SI

In the base configuration analysis, it appears clear that the main issues of the small perturbation stability are the swings caused by the inter-area mode M1 between the plant in Termini Imerese and the slack on the Italian peninsula. The damping factor of this mode is 5.66% in the *High Import* DP, below 3.88% in the *Low Load* DP, and 1.08% in the *Lines out of Service* DP.

This section aims at determining the contribution of DC-link-based SI provided by the FCWT units. The initial setting of the SI gain K_{in} (see Figure 2b) is 0; then, its value is gradually increased to 50 by steps of 5. The modal analysis is then repeated for each value of K_{in} and for each DP; for the sake of conciseness, the results are reported just for a selected number of values, i.e., K_{in} = [0, 10, 30, 50].

For the *High Import* DP, the results are shown in Table 14. Increasing the gain K_{in} provides a significant improvement to the damping ratio of mode M1. M2 and M5 experience a minor decrease in damping with increasing values of K_{in}. D1, M3, and M4 are not affected by K_{in}.

Table 14. Effect of increasing SI contribution from FCWTs on the modes of the *High Import* DP.

K_{in} (p.u.)	M1		D1		M2		M3		M4		M5	
	f (Hz)	ζ (%)	f (Hz)	ζ (%)	f (Hz)	ζ (%)	f (Hz)	ζ (%)	f (Hz)	ζ (%)	f (Hz)	ζ (%)
0	0.77	5.66	1.80	5.9	1.3	7.24	1.59	8.83	1.59	8.90	1.66	9.91
10	0.77	5.67	1.80	5.9	1.3	7.23	1.59	8.83	1.59	8.90	1.66	9.91
30	0.77	7.39	1.80	5.9	1.3	7.07	1.59	8.83	1.59	8.90	1.66	9.69
50	0.78	7.35	1.80	5.9	1.3	7.03	1.59	8.83	1.59	8.90	1.67	9.66

For the *Low Load* DP, the results are presented in Table 15. Increasing values of K_{in} provide a significant improvement to the damping ratio of mode M1, making it properly damped, a slightly detrimental effect on mode M6 and no effect whatsoever on M7.

Table 15. Effect of increasing SI contribution from FCWTs on the modes in the *Low Load* DP.

K_{in} (p.u.)	M1		M6		M7	
	f (Hz)	ζ (%)	f (Hz)	ζ (%)	f (Hz)	ζ (%)
0	0.79	3.88	1.73	7.38	1.77	7.67
10	0.79	4.37	1.73	7.34	1.77	7.67
30	0.79	5.18	1.73	7.30	1.77	7.67
50	0.79	5.37	1.73	7.28	1.77	7.67

For the *Lines out of Service* DP, the results are reported in Table 16. Increasing values of K_{in} provide a significant improvement to the damping ratio of mode M1, making it properly damped, until the value of K_{in} reaches 30, then the damping ratio of M1 becomes worst. The effect on the other two modes is the same as in the *Low Load* one.

Table 16. Effect of increasing SI contribution from FCWTs on the modes in the *Lines out of Service* DP.

K_{in} (p.u.)	M1		M6		M7	
	f (Hz)	ζ (%)	f (Hz)	ζ (%)	f (Hz)	ζ (%)
0	0.75	1.08	1.72	7.95	1.76	8.26
10	0.75	3.00	1.72	7.92	1.76	8.27
30	0.77	5.17	1.73	7.88	1.76	8.27
50	0.78	4.85	1.73	7.87	1.76	8.27

In conclusion, regarding the *Low Load* and the *Lines out of service* DPs, the SI provided by FCWT can increase the damping ratio of inter-area mode M1 to a value above the 5% threshold. However, it can do so just by a small margin. For a K_{in} value of 30, in the *Low Load* DP the damping ratio increases to a value of 5.18% and to a value of 5.17% in the *Lines out of service* DP. For this reason, in order to guarantee a more comfortable margin, other measures must be implemented. As shown in the following, tuning the PSS of the plants mainly involved in mode M1 allows to increase this margin to a more comfortable level.

4.2.3. Combined Configuration

A separate analysis has shown how values of the gain of the PSS of the TIMP plant ranging from 0.5 to 1 p.u. can provide satisfactory damping to inter-area mode M1 without compromising the stability of the local modes. For the *High Import* DP, the damping ratio gets above 10% and between 5 and 10% for the *Low Load* and *Lines out of Service* DP.

In this subsection, the combined influence of the FCWT frequency support schemes and the PSS tuning is investigated. For the FCWT units, the SI gain value of K_{in} = 30 p.u. is selected; for the PSS in TIMP, the value of the gain equal to 1 p.u is adopted.

The results reported in the following tables show that a combined effort from RES and PSS allows very good damping improvement for all the modes, even above the conservative

threshold of 10%. In particular, this is true for the critical inter-area mode M1. For the *High Import* DP, the results are presented in Table 17.

Table 17. Electromechanical comparison between the base case and the combined contribution of RESs frequency support and PSS tuning to the small signal stability for the *High Import* DP. Check marks indicate those modes with a damping factor greater than 10%.

Case	M1		D1		M2		M3		M4		M5	
	f (Hz)	ζ (%)	f (Hz)	ζ (%)	f (Hz)	ζ (%)	f (Hz)	ζ (%)	f (Hz)	ζ (%)	f (Hz)	ζ (%)
Base	0.77	5.66	1.80	5.9	1.3	7.24	1.59	8.83	1.59	8.90	1.66	9.91
Comb.	✓	✓	1.80	5.9	✓	✓	✓	✓	✓	✓	✓	✓

For the *Low Load* DP, the results are presented in Table 18. It can be seen how, with a combined effort, the critical inter-area mode is properly stabilized and damped above the 10% threshold. On the other hand, modes M6 and M7, due to the size and the location of the plants involved, are not significantly affected; nonetheless maintain a damping ratio above 5%.

Table 18. Comparison between the base case and the combined contribution of RESs frequency support and PSS tuning to the small signal stability for the *Low Load* DP. Check marks indicate those modes with a damping factor greater than 10%.

Case	M1		M6		M7	
	f (Hz)	ζ (%)	f (Hz)	ζ (%)	f (Hz)	ζ (%)
Base	0.79	3.88	1.73	7.38	1.77	7.67
Combined	✓	✓	1.73	7.30	1.77	7.68

For the *Line out of services* DP, the results are presented in Table 19. This DP is a variation of the *Low Load* one, and the conclusions are very similar.

Table 19. Comparison between the base case and the combined contribution of RESs frequency support and PSS tuning to the small signal stability for the *Lines out of Service* DP. Check marks indicate those modes with a damping factor greater than 10%.

Case	M1		M6		M7	
	f (Hz)	ζ (%)	f (Hz)	ζ (%)	f (Hz)	ζ (%)
Base	0.75	1.08	1.72	7.95	1.76	8.26
Combined	✓	✓	1.73	7.88	1.76	8.27

The results show how the Sicilian grid forecasted for 2050 presents good damping of oscillatory modes and displays a variety of tools to tackle frequency instabilities. For every identified DP a modal analysis was performed. The *High Export*, *High Load*, and *Island* DPs do not present any electromechanical modes with a damping ratio below 10%. The *High Import*, *Low Load*, and *Lines out of Service* DP present some local or intra-plant modes that are stable and one inter-area mode with the peninsula, which is either barely stable or unstable. This inter-area mode, between Sicily and the Italian peninsula, is the main concern for the small perturbation stability. It was shown how it can be properly damped thanks to the contribution of SI provided by FCWT and tuning the PSS of the plant in Termini Imerese.

In conclusion, the amount of RES forecasted for the year 2050 does not compromise the small signal stability of the Sicilian grid; on the contrary, it provides a variety of tools to enhance it.

5. Voltage Stability Analysis

This last section presents the results of the voltage stability analysis. The voltage stability analysis consists of a steady-state analysis (i.e., slow dynamics) to identify the maximum loading conditions keeping acceptable voltages at all busses, i.e., between the 0.9 and the 1.1 of the per-unit rated voltage.

First, the voltage stability analysis was carried out considering the reactive support given only by the synchronous generators in service. Then, the RES power plants were equipped with the specifications adopted by Terna in the Italian grid code [53–55] for the reactive provision, and the second set of tests was carried out. Finally, a sensitivity analysis of the parameters of the RES reactive controllers was performed to improve the voltage levels in particularly weak grid conditions.

5.1. Procedure

The PV curve calculation tool of DIgSILENT was used and adapted for this task to carry out the voltage stability analysis. Basically, we found the critical points of voltage instability by increasing the power demand of loads (zero and negative loads have not been considered for this evaluation) until the load flow calculation no longer converges. In particular, the HV voltage magnitudes were monitored to fulfil the 0.9–1.1 p.u. limits.

Reactive support of the RES was also considered and the current capability limits given by Terna in [53,54] were used as reference (Figure 16a, red solid line). The maximum/minimum reactive support must be equal to ±35% of the currently active power available. Regarding the controller logic, the injection of reactive power, depending on the voltage values, was assumed to be in accordance with Figure 16b, where $|\Delta V_{max}| = |\Delta V_{min}| = 0.05 \cdot V_{nom}$:

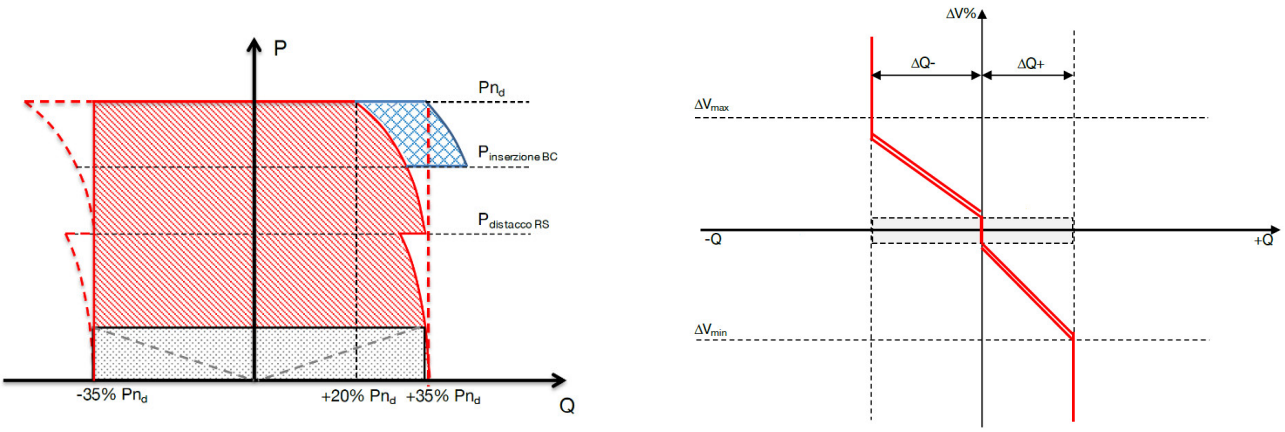

(**a**) (**b**)

Figure 16. Capability curve implemented for wind and PV plants (**a**) [53,54], Q/V curve given by Terna in [54] (**b**).

According to the annexes [53] and [54], the reactive droop was set equal to 14%:

$$droop = \frac{\Delta V}{\Delta Q} = \frac{|0.05|}{|0.35|} = 14\% \tag{11}$$

In its base case, the Sicilian grid presents a quite high loadability margin, equal to 65%. However, for our studies, a loadability equal to/higher than 40% is also considered acceptable.

5.2. Results

The *base configuration* results are first analyzed, where only the synchronous machines provide reactive support. These preliminary results are not realistic, but they can be used

as a first insight and benchmark for the subsequent assessments. Then, a second study was performed considering the reactive contribution given by the RES and BESS [55] as well. The analysis was stopped as soon as the voltage profile of one single HV busbar goes below the lower 0.9 limit. The 2050 DPs present a quite low percentage of synchronous machines: hence, a higher voltage instability is expected.

The results are summarized in Table 20 (the critical DPs are highlighted in bold), along with the loadability margin in MW and percentage. It can be easily appreciated that the *High Import* and *Island* DPs present the lowest loadability margins, less than 15% and, along with loadability of the *High Load* one, they are much lower than the adopted threshold of 40%: additional resources must be here employed to increase voltage stability margins since the synchronous machines only are not enough to guarantee a satisfactory stability level. The remaining DPs already present enough loadability.

Table 20. Loadability margins for the selected DPs.

Dispatching Profile	Initial Load (MW)	Final Load (MW)	Loadability (MW)	Loadability (%)
High Export	1835	3717	1882	102.5
High Import	**3220**	**3596**	**376**	**11.7**
High Load	4088	5498	1410	34.5
Low Load	1510	3346	1836	121.5
Island	**4289**	**4857**	**568**	**13.2**
Lines out of service	1510	3225	1715	113.5

5.2.1. High Import and Island Dispatching Profiles

The voltage profiles of the 400 kV busbars of the *High Import* DP are shown in Figure 17a, starting from the initial demand of 3220 MW; the maximum demand achievable is equal to 3596 MW. The voltage profiles of the 400 kV busbars of the *Island* DP are shown in Figure 17b, starting from the initial demand of 4289 MW; the maximum demand achievable is equal to 4857 MW.

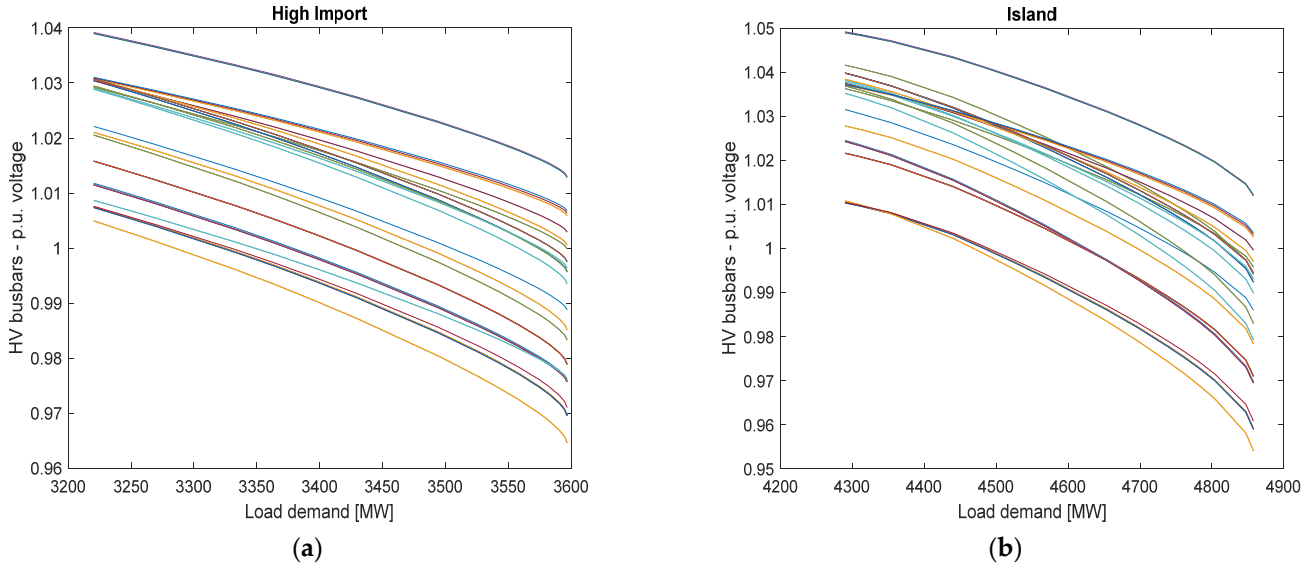

(**a**) (**b**)

Figure 17. HV voltage profile of the *High Import* DP (**a**), HV voltage profile of the *Island* DP (**b**).

5.2.2. RES Contribution

The reactive contribution of the RES was considered in the voltage stability analysis. All the HV connected wind plants, the photovoltaic plants connected to the HV and MV network, representing the MV dispersed generation, and the BESS were modified to provide reactive power support. All the inverters were set up with the current Italian standards

as described. Since a low level of loadability was detected, analysis was carried out to maximize the reactive support with no restrictions for the inverters: they can provide their full capability and hence overreach the existing limits given by Terna in [53–55].

The results are shown in Table 21. This solution, with "full inverters capability", offers quite satisfactory results compared to the base case, as in all the DPs the margin is increased. Despite this, in the *High Import* and *Island* ones, the loadability is still too low and hence cannot be considered acceptable, even if it is almost doubled compared to the *base configuration*. The *High load* profile reached an acceptable margin instead.

Table 21. Loadability margins for the selected DPs with the full RES reactive contribution.

Dispatching Profile	Initial Load (MW)	Loadability (MW)	Loadability (%)	Loadability Base Case (%)
High Export	4592	2757	150.2	102.5
High Import	**3993**	**773**	**24.0**	**11.7**
High Load	5702	1614	40.0	34.5
Low Load	4887	3376	223.5	121.5
Island	**5791**	**1502**	**35.0**	**13.2**
Lines out of service	4615	3105	205.5	113.5

5.2.3. Critical Dispatching Profiles

Analyzing the results, in both the *High Import* and *Island* DPs, the "critical busses" are two HV nodes close to Priolo, where two large thermal plants are nowconnected, but will be considered decommissioned in 2050: Erg Nuce Nord and Priolo Gargallo. For the *High Import* profile, the critical node is the PRGP busbar, and for the *Island* one, the EGNP busbar, both connected to the HV 150 kV substation of Melilli, which is the interconnection with the 230 and 400 kV lines.

According to this analysis, the synchronous machines of the Priolo power plants (four machines of the Erg Nuce Nord and two for the Priolo Gargallo (PRGP)) were assumed as still in operation as synchronous condensers only to guarantee suitable reactive support. This solution is cheap, reasonable, and already acceptable since Terna is managing to install synchronous condensers in a few old thermal plants in the south of Italy to provide inertia and voltage control to stabilize the grid.

Assuming the full reactive capability of the RES converters and thanks to the Priolo compensators, the loadability can be increased for the *Island* DP up to 40% (Figure 18a), and for the *High Import* DP up to 60% (Figure 18b):

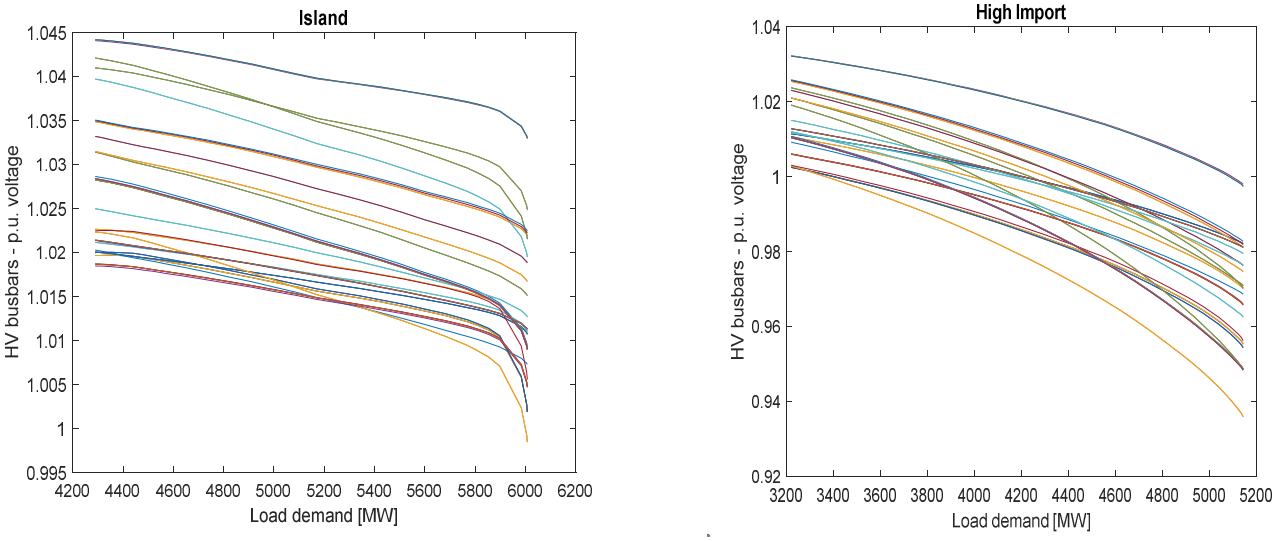

(**a**) (**b**)

Figure 18. HV voltage profile of the *Island* DP (**a**), HV voltage profile of the *High Import* DP (**b**).

The results are summarized in the following table (Table 22, where the improvements are highlighted): for all the other DPs, the Priolo compensators can be kept off, as they already present reasonable loadability margins.

Table 22. Loadability margins for the selected DPs for 2050 with a full RES reactive contribution at Priolo as a synchronous compensator.

Dispatching Profile	Final Load (MW)	Loadability (MW)	Loadability (%)	Loadability without Priolo (%)
High Import	5144	1924	60.0	24.0
Island	6007	1718	40.0	35.0

A second analysis was carried out to better investigate the problem, where the power plants in Priolo were completely dismantled and the connection busses employed for the connection of wind turbine parks, hence taking advantage of the already existing infrastructures. The new wind turbines were connected to the grid through PWM converters, able to provide reactive power. The capability has again been extended up to the maximum available to maximize the reactive support (previously defined as "full inverters capability"). The loadability margins were recalculated: the results are shown in Table 23.

Table 23. Loadability margins for the selected DPs for 2050 with a full RES reactive contribution of Priolo as wind park.

Dispatching Profile	Final Load (MW)	Loadability (MW)	Loadability (%)	Loadability without Priolo (%)
High Import	5625	2405	74.6	24.0
Island	6036	1747	41.0	35.0

Thanks to the larger reactive capability provided by the converters, the *High Import* DP can reach a satisfactory loadability level equal to 75%, while in the *Island* one is increased by few MW up to a final 41%. Anyway, this latest value can be considered suitable for grid stability and the analysis can now be considered settled.

It has been noticed that when Sicily is importing power from continental Italy, it is facing a high-power demand or it is even not connected, its loadability margin, and hence its voltage stability is reduced. The capability of the static converters has been extended up to the maximum available, supporting the voltage stability to a satisfactory level. For the *Island* and *High Import* DPs the local reactive compensation at the Priolo substation allows increasing the loadability margin. Sicily does not present a good loadability margin in the base case, with both the combination of synchronous generators and RES plants equipped with the current reactive settings [53,54]. However, the presence of RES plant with "full inverters capability", along with specific compensation in local substations, improves the voltage stability and guarantees the voltage security of the power system.

6. Conclusions

This paper reports the results of a dynamic analysis carried out by EnSiEL for WP1 of the OSMOSE project (Task 1.4.3) concerning the feasibility of some of the scenarios and DPs identified for 2050 in Task 1.1 and Task 1.2, in the particular case of the power system of Sicily, one of the two main islands of Italy.

In particular, EnSiEL has assessed some typical perturbations of power systems, e.g., loss of a large generator, slow increase in loads, or contingencies of branches. These simulations were performed on a dedicated large grid model of the electrical network of Sicily, provided by Terna, the Italian TSO. This grid model was updated according to both the capacities defined by the scenarios provided by Task 1.1 and the system-wide balancing of energy supply and demand identified area by area by Task 1.2. Therefore, Task 1.4.3 has evaluated if the outputs of the above-mentioned Tasks are feasible from a

dynamic point of view, identified possible lack of stability, and, in such a case, suggested possible countermeasures, picking up any flexibility resource that can be useful.

The analysis has regarded angle stability under large and small perturbations and voltage stability. Table 24 reports the conclusions and indications drawn for each DP with respect to the three types of stability.

Table 24. Conclusions summary.

Type of Stability	Is Stability Guaranteed?	Does the Operational Condition Need Specific Additional Flexibilitiy Tools?	Solutions Identified/Notes
High Export DP			
Large perturbation angle stability	YES	YES	DSR [1] and BESS FCR [2] are required to guarantee the normal operating conditions
Small perturbation angle stability	YES	NO	-
Voltage stability	YES	YES	Extend the reactive capability of RES units
High Import DP			
Large perturbation angle stability	NO	YES	DSR and BESS FCR are required
Small perturbation angle stability	YES	YES	SI [3] by FCWTs [4] and PSS tuning are required
Voltage stability	NO	YES	Extend the reactive capability of RES units + Local compensation in Priolo substation
High Load DP			
Large perturbation angle stability	YES	NO	-
Small perturbation angle stability	YES	NO	-
Voltage stability	NO	YES	Extend the reactive capability of RES units
Island DP			
Large perturbation angle stability	NO	YES	DSR and BESS FCR are required
Small perturbation angle stability	YES	NO	-
Voltage stability	NO	YES	Extend the reactive capability of RES units + Local compensation in Priolo substation
Low Load DP			
Large perturbation angle stability	NO	YES	DSR and BESS FCR are required
Small perturbation angle stability	NO	YES	SI by FCWTs and PSS tuning are required
Voltage stability	YES	YES	Extend the reactive capability of RES units
Lines out of service DP			
Large perturbation angle stability	NO	YES	DSR and BESS FCR are required
Small perturbation angle stability	NO	YES	SI by FCWTs and PSS tuning are required
Voltage stability	YES	YES	Extend the reactive capability of RES units

[1] Demand-Side Response; [2] Frequency Containment Reserve; [3] Synthetic Inertia; [4] Full-Converter Wind Turbines.

Results show that large-perturbation angle stability is guaranteed in all the DPs and for all events, except for a very unlikely operating condition that results in a high import power loss. However, it is possible to achieve stability in such a critical operating condition, taking into account the contribution of BESSs and/or DSR, which results to be mandatory. As for the post fault steady state, the contribution to frequency regulation of BESSs and/or DSR is generally sufficient to keep frequency in the range 49.9–50.1 Hz. In only two cases, this has resulted not been possible; however, this constraint can be managed by subsequent control actions.

Regarding small-perturbation angle stability, for the DPs in which RES support frequency control is not active, in some cases, low damped electromechanical modes are present. In particular, the interarea mode can be stabilized thanks to the contribution of SI provided by wind farms and by suitably tuning the PSSs of the relevant generators. Therefore, thanks to the availability of SI, the Sicilian grid shows strong small perturbation stability features.

Finally, simulations assessing the voltage stability were first performed considering only the synchronous generator's reactive contribution and then the RES support as well. Because of the high penetration of RESs in 2050, high voltage instability is observed unless flexibility provided by RES is considered. Indeed, exploiting the reactive contribution of RESs voltage stability is guaranteed in all the studied operating conditions.

Despite that the analysis provided in this paper covers many stability issues, considering a complete set of flexibility options with a detailed model of a real power system, further analyses should be conducted to confirm the conclusions we have obtained. First of all, grid portions different from the one of Sicily should be considered. Moreover, further stability aspects should be analyzed, focusing on time scales lower than the one of electromechanical phenomena considered in this work. Indeed, the high penetration of converters may introduce stability issues not taken into account till today by conventional power system analysis and this will be related to high-frequency dynamics, such as the ones associated with the switching of converters. Future works will be thus dedicated to extend our stability analysis by considering power systems different from the one of Sicily and using models able to capture the dynamics at time scales lower than the electrochemical phenomena.

Author Contributions: Conceptualization: A.B.; methodology: A.B., F.C., F.D., V.I., F.N. and A.V.; data curation: A.V.; software: J.A.A., F.C., F.D., V.I., T.P. and A.V.; validation: J.A.A., F.C., T.P. and A.V.; writing—original draft preparation: J.A.A., F.C., T.P. and A.V.; writing—review and editing: A.B., F.D., V.I. and F.N.; supervision: A.B. and F.N. All authors have read and agreed to the published version of the manuscript.

Funding: This work is part of the OSMOSE project. It has received funding from the European Union's Horizon 2020 research and innovation program under grant agreement n. 773406.

Institutional Review Board Statement: Not applicable.

Informed Consent Statement: Not applicable.

Data Availability Statement: Not applicable.

Conflicts of Interest: The authors declare no conflict of interest. The funders had no role in the design of the study; in the collection, analyses, or interpretation of data; in the writing of the manuscript, or in the decision to publish the results.

References

1. OSMOSE—Optimal System-Mix of Flexibility Solutions for European Flexibility. Available online: https://www.osmose-h2020.eu (accessed on 26 April 2022).
2. Liu, H.; Yang, S.; Yuan, X. Inertia Control Strategy of DFIG-Based Wind Turbines Considering Low-Frequency Oscillation Suppression. *Energies* **2022**, *15*, 29. [CrossRef]
3. Wang, J.; Xu, Y.; Wu, X.; Huang, J.; Zhang, X.; Yuan, H. Enhanced Inertial Response Capability of a Variable Wind Energy Conversion System. *Energies* **2021**, *14*, 8132. [CrossRef]

4. Li, Y.; Xu, Z.; Wong, K.P. Advanced Control Strategies of PMSG-Based Wind Turbines for System Inertia Support. *IEEE Trans. Power Syst.* **2017**, *32*, 3027–3037. [CrossRef]
5. Xu, Y.; Chen, P.; Zhang, X.; Yang, D. An Improved Droop Control Scheme of a Doubly-Fed Induction Generator for Various Disturbances. *Energies* **2021**, *14*, 7980. [CrossRef]
6. Bolzoni, A.; Terlizzi, C.; Perini, R. Analytical Design and Modelling of Power Converters Equipped with Synthetic Inertia Control. In Proceedings of the 2018 20th European Conference on Power Electronics and Applications (EPE'18 ECCE Europe), Riga, Latvia, 17–21 September 2018; pp. 1–10.
7. Fang, J.; Zhang, R.; Li, H.; Tang, Y. Frequency Derivative-based Inertia Enhancement by Grid-Connected Power Converters with a Frequency-Locked-Loop. *IEEE Trans. Smart Grid* **2018**, *10*, 4918–4927. [CrossRef]
8. Conte, F.; Massucco, S.; Silvestro, F. Frequency control services by a building cooling system aggregate. *Electr. Power Syst. Res.* **2016**, *141*, 137–146. [CrossRef]
9. Tindemans, S.H.; Strbac, G. Low-Complexity Decentralized Algorithm for Aggregate Load Control of Thermostatic Loads. *IEEE Trans. Ind. Appl.* **2021**, *57*, 987–998. [CrossRef]
10. Trovato, V.; Sanz, I.M.; Chaudhuri, B.; Strbac, G. Advanced Control of Thermostatic Loads for Rapid Frequency Response in Great Britain. *IEEE Trans. Power Syst.* **2017**, *32*, 2106–2117. [CrossRef]
11. Lin, Y.; Barooah, P.; Meyn, S.; Middelkoop, T. Experimental evaluation of frequency regulation from commercial building HVAC systems. *IEEE Trans. Smart Grid* **2015**, *6*, 776–783. [CrossRef]
12. Cheng, B.; Powell, W.B. Co-Optimizing Battery Storage for the Frequency Regulation and Energy Arbitrage Using Multi-Scale Dynamic Programming. *IEEE Trans. Smart Grid* **2018**, *9*, 1997–2005. [CrossRef]
13. Zhao, H.; Wu, Q.; Hu, S.; Xu, H.; Rasmussen, C.N. Review of energy storage system for wind power integration support. *Appl. Energy* **2015**, *137*, 545–553. [CrossRef]
14. Conte, F.; Massucco, S.; Schiapparelli, G.P.; Silvestro, F. Day-ahead and intra-day planning of integrated BESS-PV systems providing frequency regulation. *IEEE Trans. Sustain. Energy* **2020**, *11*, 1797–1806. [CrossRef]
15. Berizzi, A.; Bovo, C.; Ilea, V.; Merlo, M.; Miotti, A.; Zanellini, F. Decentralized reactive power control of wind power plants. In Proceedings of the 2012 IEEE International Energy Conference and Exhibition, ENERGYCON 2012, Florence, Italy, 9–12 September 2012.
16. Christakou, K.; Tomozei, D.C.; Bahramipanah, M.; Le Boudec, J.Y.; Paolone, M. Primary voltage control in active distribution networks via broadcast signals: The case of distributed storage. *IEEE Trans. Smart Grid* **2014**, *5*, 2314–2325. [CrossRef]
17. Ilea, V.; Bovo, C.; Falabretti, D.; Merlo, M.; Arrigoni, C.; Bonera, R.; Rodolfi, M. Voltage control methodologies in active distribution networks. *Energies* **2020**, *13*, 3293. [CrossRef]
18. Ma, K.; Yao, T.; Yang, J.; Guan, X. Residential power scheduling for demand response in smart grid. *Int. J. Electr. Power Energy Syst.* **2016**, *78*, 320–325. [CrossRef]
19. Bañales, S.; Dormido, R.; Duro, N. Smart Meters Time Series Clustering for Demand Response Applications in the Context of High Penetration of Renewable Energy Resources. *Energies* **2021**, *14*, 3458. [CrossRef]
20. Wang, J.; Padullaparti, H.; Ding, F.; Baggu, M.; Symko-Davies, M. Voltage Regulation Performance Evaluation of Distributed Energy Resource Management via Advanced Hardware-in-the-Loop Simulation. *Energies* **2021**, *14*, 6734. [CrossRef]
21. Stephen, A.A.; Musasa, K.; Davidson, I.E. Voltage Rise Regulation with a Grid Connected Solar Photovoltaic System. *Energies* **2021**, *14*, 7510. [CrossRef]
22. Szultka, A.; Szultka, S.; Czapp, S.; Karolak, R.; Andrzejewski, M.; Kapitaniak, J.; Kulling, M.; Bonk, J. Voltage Profiles Improvement in a Power Network with PV Energy Sources—Results of a Voltage Regulator Implementation. *Energies* **2022**, *15*, 723. [CrossRef]
23. Ding, Z.; Huang, X.; Liu, Z. Active Exploration by Chance-Constrained Optimization for Voltage Regulation with Reinforcement Learning. *Energies* **2022**, *15*, 614. [CrossRef]
24. Li, W.; Tang, M.; Zhang, X.; Gao, D.; Wang, J. Operation of Distributed Battery Considering Demand Response Using Deep Reinforcement Learning in Grid Edge Control. *Energies* **2021**, *14*, 7749. [CrossRef]
25. Weibezahn, J.; Göke, L.; Orrù, L. OSMOSE D1.1: European Long-Term Scenarios Description. 2019. Available online: https://www.osmose-h2020.eu/download/d1-1-european-long-term-scenarios-description (accessed on 29 March 2022).
26. Weibezahn, J.; Göke, L.; Poli, D.; Protard, V.; Bourien, Y.M.; Ažman, G. OSMOSE D1.2: Flexibility Cost and Operational Data Outlook. 2020. Available online: https://www.osmose-h2020.eu/download/d1-2-flexibility-cost-and-operational-data-outlook (accessed on 29 March 2022).
27. Bourmaud, J.-Y.; Lhuillier, N.; Orlic, D.; Kostic, M.; Heggarty, T.; Grisey, N. OSMOSE D1.3: Optimal Mix of Flexibility. 2022. Available online: https://www.osmose-h2020.eu/wp-content/uploads/2022/04/D1.3-Optimal-Mix-of-Flexibility-1.pdf (accessed on 29 March 2022).
28. ENSIEL. Available online: https://www.consorzioensiel.it (accessed on 28 February 2022).
29. Heggarty, T.; Bourmaud, J.Y.; Girard, R.; Kariniotakis, G. Quantifying power system flexibility provision. *Appl. Energy* **2020**, *279*, 115852. [CrossRef]
30. Berizzi, A.; Ilea, V.; Vicario, A.; Conte, F.; Massucco, S.; Adu, J.A.; Nucci, C.A.; Pontecorvo, T. Stability analysis of the OSMOSE scenarios: Main findings, problems, and solutions adopted. In Proceedings of the 2021 AEIT International Annual Conference (AEIT), Milan, Italy, 4–8 October 2021; pp. 1–6.
31. DIgSILENT GmbH. *DIgSILENT PowerFactory, User Manual*; Version 20; DIgSILENT GmbH: Gomaringen, Germany, 2019.

32. Kundur, P. *Power System Stability And Control*; McGraw-Hill: New York, NY, USA, 1994.
33. Adrees, A.; Milanović, J.V.; Mancarella, P. Effect of inertia heterogeneity on frequency dynamics of low-inertia power systems. *IET Gener. Transm. Distrib.* **2019**, *13*, 2951–2958. [CrossRef]
34. IEEE/NERC. Task Force on Short-Circuit and System Performance Impact of Inverter Based Generation. In *Impact of Inverter Based Generation on Bulk Power System Dynamics and Short-Circuit Performance*; IEEE: Piscataway, NJ, USA, 2018.
35. Eftekharnejad, S.; Vittal, V.; Heydt, G.T.; Keel, B.; Loehr, J. Small signal stability assessment of power systems with increased penetration of photovoltaic generation: A case study. *IEEE Trans. Sustain. Energy* **2013**, *4*, 960–967. [CrossRef]
36. Map of the Sicilian 380–220 kV System. Available online: http://www.regione.sicilia.it (accessed on 28 February 2022).
37. EC Directive (EU). 2018/2001 of the European Parliament and of the Council of 11 December 2018 on the promotion of the use of energy from renewable sources. *Off. J. Eur. Union* **2018**, *2001*, 1–128.
38. TERNA S.p.A. Grid Code Annexes 11, "Criteri Generali per la Taratura delle Protezione delle Reti a Tensione Uguale o Superiore a 110 kV". 2018. Available online: https://download.terna.it/terna/0000/0105/28.pdf (accessed on 29 March 2022). (In Italian)
39. TERNA S.p.A. GAUDI' Portal. Available online: https://www.terna.it/it/sistema-elettrico/gaudi (accessed on 28 February 2022).
40. Western Electricity Coordinating Council Modeling and Validation Work Group. *WECC Renewable Energy Modeling Task Force WECC Solar Plant Dynamic Modeling Guidelines*; World Environment Center: Washington, DC, USA, 2014.
41. TERNA S.p.A. Grid Code Annexes 12, "Criteri di Taratura dei Relè di Frequenza del Sistema Elettrico e Piano di Alleggerimento". 2018. Available online: https://download.terna.it/terna/0000/1127/88.pdf (accessed on 29 March 2022). (In Italian).
42. Berizzi, A.; Bosisio, A.; Ilea, V.; Marchesini, D.; Perini, R.; Vicario, A. Analysis of Synthetic Inertia Strategies from Wind Turbines for Large System Stability. In *IEEE Transactions on Industry Applications*; IEEE: New York, NY, USA, 2022. [CrossRef]
43. Wang, B.; Ni, J.; Geng, J.; Lu, Y.; Dong, X. Arc flash fault detection in wind farm collection feeders based on current waveform analysis. *J. Mod. Power Syst. Clean Energy* **2017**, *5*, 211–219. [CrossRef]
44. Bolzoni, A.; Perini, R. Experimental validation of a novel angular estimator for synthetic inertia support under disturbed network conditions. In Proceedings of the 2019 21st European Conference on Power Electronics and Applications (EPE'19 ECCE Europe), Genova, Italy, 3–5 September 2019; pp. 1–10. [CrossRef]
45. Hu, J.; Huang, Y.; Wang, D.; Yuan, H.; Yuan, X. Modeling of grid-connected DFIG-based wind turbines for dc-link voltage stability analysis. *IEEE Trans. Sustain. Energy* **2015**, *6*, 1325–1336. [CrossRef]
46. Adu, J.A.; Napolitano, F.; Nucci, C.A.; Diego Rios Penaloza, J.; Tossani, F. A DC-Link Voltage Control Strategy for Fast Frequency Response Support. In Proceedings of the 2020 IEEE 20th Mediterranean Electrotechnical Conference (MELECON), Palermo, Italy, 16–18 June 2020; pp. 470–475. [CrossRef]
47. Adu, J.A.; Rios Penaloza, J.D.; Napolitano, F.; Tossani, F. Virtual Inertia in a Microgrid with Renewable Generation and a Battery Energy Storage System in Islanding Transition. In Proceedings of the SyNERGY MED 2019—1st International Conference on Energy Transition in the Mediterranean Area, Cagliari, Italy, 28–30 May 2019.
48. ENTSO-E. Demand Connection Code. Available online: https://www.entsoe.eu/major-projects/network-code-development/demand-connection (accessed on 20 June 2020).
49. TERNA S.p.A. Codice di trasmissione, Dispacciamento, Sviluppo e Sicurezza Della Rete. 2018. Available online: https://download.terna.it/terna/0000/0107/31.pdf (accessed on 29 March 2022). (In Italian)
50. ENTSO-E. *Frequency Stability Evaluation Criteria for the Synchronous Zone of Continental Europe: Requirements and Impacting Factors*; ENTSO-E: Brussels, Belgium, 2016.
51. Machowski, J.; Bialek, J.W.; Bumby, J.R. *Power System Dynamics: Stability and Control*; John Wiley & Sons: Hoboken, NJ, USA, 2008; ISBN 9780470725580.
52. Gonzalez-Longatt, F.; Rueda, J. *PowerFactory Applications for Power System Analysis*; Springer: Berlin/Heidelberg, Germany, 2014; ISBN 978-3-319-12957-0.
53. TERNA S.p.A. Grid Code Annexes 17, "Centrali Eoliche—Condizioni Generali di Connessione Alle Reti AT. Sistemi di Protezione, Regolazione e Controllo". 2019. Available online: https://download.terna.it/terna/0000/0105/34.pdf (accessed on 29 March 2022). (In Italian)
54. TERNA S.p.A. Grid Code Annexes 68, "Centrali Fotovoltaiche—Condizioni Generali di Connessione Alle Reti AT. Sistemi di Protezione, Regolazione e Controllo". 2019. Available online: https://download.terna.it/terna/0000/0105/84.pdf (accessed on 29 March 2022). (In Italian)
55. CEI 0–16. *Regola Tecnica di Riferimento per la Connessione di Utenti Attivi e Passivi Alle Reti AT ed MT Delle Imprese Distributrici di Energia Elettrica*; Comitato Elettrico Italiano: Milano, Italy, 2019. (In Italian)